2mit

NASA TECHNICAL NOTE

NASA TN D-7525

TN D-7525

INTERFERENCE BETWEEN EXHAUST SYSTEM AND AFTERBODY OF TWIN-ENGINE FUSELAGE CONFIGURATIONS

by Jack F. Runckel

Langley Research Center
Hampton, Va. 23665

NATIONAL AERONAUTICS AND SPACE ADMINISTRATION • WASHINGTON, D. C. • MAY 1974

1. Report No. NASA TN D-7525	2. Government Accession No.	3. Recipient's Catalog No.
4. Title and Subtitle INTERFERENCE BETWEEN EXHAUST SYSTEM AND AFTERBODY OF TWIN-ENGINE FUSELAGE CONFIGURATIONS		5. Report Date May 1974 6. Performing Organization Code
7. Author(s) Jack F. Runckel		8. Performing Organization Report No. L-9283 10. Work Unit No. 501-24-06-01
9. Performing Organization Name and Address NASA Langley Research Center Hampton, Va. 23665		11. Contract or Grant No. 13. Type of Report and Period Covered Technical Note
12. Sponsoring Agency Name and Address National Aeronautics and Space Administration Washington, D.C. 20546		14. Sponsoring Agency Code

15. Supplementary Notes

16. Abstract

Some of the mutual aircraft afterbody and engine nozzle interferences that can exist on aircraft complex aft-ends and on simplified twin-jet afterbodies are reviewed. Emphasis is placed on studies of twin-engine fuselage configurations with nozzles installed near the terminus of the afterbody where the interactions of the nozzle exhausts and external stream produce a complex flow-field environment. The magnitude of the aft-end problem for real aircraft configurations is illustrated, and some theoretical and empirical considerations of afterbody drag on simple bodies are treated. Many of the factors regarding airframe-installation effects on nozzle performance are discussed, as well as nozzle-installation effects on aircraft performance.

17. Key Words (Suggested by Author(s))	18. Distribution Statement
Propulsion systems Aerodynamics	Unclassified – Unlimited STAR Category 28

19. Security Classif. (of this report)	20. Security Classif. (of this page)	21. No. of Pages	22. Price*
Unclassified	Unclassified	44	$3.25

*For sale by the National Technical Information Service, Springfield, Virginia 22151

CONTENTS

INTERFERENCE BETWEEN EXHAUST SYSTEM AND AFTERBODY OF TWIN-ENGINE FUSELAGE CONFIGURATIONS

By Jack F. Runckel
Langley Research Center

SUMMARY

This paper reviews some of the mutual aircraft afterbody and engine nozzle interferences that can exist on aircraft complex aft-ends and on simplified twin-jet afterbodies. Information was obtained at the NASA Langley Research Center from numerous investigations of jet interference on experimental models at subsonic, transonic, and supersonic speeds. Emphasis is placed on studies of twin-engine fuselage configurations with nozzles installed near the terminus of the afterbody where the interactions of the nozzle exhausts and external stream produce a complex flow-field environment. Airframe interferences on nozzle performance considered are: installation locations in the afterbody, boattailing ahead of the nozzles, and effects of the tails and protuberances. Airframe interference on nozzle performance may be either detrimental or favorable, depending on the particular installation. The effect on afterbody drag of nozzle-exit axial location appears to pose more problems than the lateral spacing of the nozzles. For closely spaced nozzles, the shape of the interfairing between the nozzles has a pronounced effect on afterbody nozzle performance. Jet induced forces on the afterbody and nozzles can be of opposite sign so that meaningful aft-end measurements should include the sum of the afterbody-plus-nozzle forces.

INTRODUCTION

The development of new military aircraft has focused attention on the need for research on the back-end problems of airframe-engine nozzle integration. This area has become especially critical because of the requirements for multimission aircraft to operate effectively at subsonic, transonic, and supersonic speeds. A primary consideration is the prediction of drag for designs which have engines installed in close proximity to the empennage. Considerable effort has been expended in examining the procedures for installing the rear engines in the airframe (refs. 1 to 6). The present paper is intended as a brief summary of some of the features concerning aircraft-engine integration that have been found from research conducted at the NASA Langley Research Center. Experimental results are used to provide examples of mutual interaction between the

engine exhaust system and the airframe afterbody. Because of the complex flow environment the performance of aircraft afterbodies is generally not amenable to analytical studies. Consequently, wind-tunnel experimental data must be used to understand and provide the basis for estimating the afterbody contribution to aircraft drag. However, the present paper utilizes some simplified analytical methods as a guide to help in directing analysis of the experimental results.

Some examples are included to illustrate the nature of the boattail drag problem and the factors contributing to the disproportionate share of the drag that can exist in an afterbody region. It should be emphasized that many of the experimental results presented herein were obtained on relatively simple and clean afterbody configurations to indicate performance trends due to parametric variations. Some of the effects of real aircraft aft-ends are included where the local flow fields are much more complex and where component interferences exist. These complications result in large reductions in performance compared with those of isolated aft-end models.

SYMBOLS

A_{max} maximum cross-sectional area of body

C_D drag coefficient, $\frac{\text{Drag}}{q_\infty A_{max}}$

$C_{D,a}$ afterbody drag coefficient, $\frac{D_a}{q_\infty A_{max}}$

$C_{D,a+n}$ afterbody-plus-nozzle drag coefficient, $\frac{D_{a+n}}{q_\infty A_{max}}$

$C_{D,f}$ friction drag coefficient, $\frac{D_f}{q_\infty A_{max}}$

$C_{D,p}$ pressure drag coefficient, $\frac{D_p}{q_\infty A_{max}}$

$C_{D,w}$ wave drag coefficient, $\frac{D_w}{q_\infty A_{max}}$

$C_{D,\beta}$ boattail pressure drag coefficient

C_p pressure coefficient, $\frac{p - p_\infty}{q_\infty}$

$C_{p,b}$ base pressure coefficient, $\frac{p_b - p_\infty}{q_\infty}$

D_a drag on afterbody

D_{a+n}	drag on afterbody and nozzles
D_f	friction drag
D_n	drag on nozzles
D_p	pressure drag
D_w	wave drag
d_e	nozzle exit diameter
d_m	model maximum diameter
d_n	nozzle maximum diameter
F_i	isentropic gross thrust of nozzles
F_j	measured jet (gross) thrust of nozzles
h	distance normal from body
L	model length
l	afterbody length
M	free-stream Mach number
p	local static pressure
p_b	interfairing base static pressure
$p_{t,j}$	jet total pressure
$p_{t,l}$	local total pressure
$p_{t,\infty}$	free-stream total pressure
p_∞	free-stream static pressure

q_∞ free-stream dynamic pressure

s distance between engine center lines

x distance from model nose

β_a afterbody boattail angle ahead of nozzle, deg

β_n nozzle boattail angle, deg

$\frac{\Delta(F_j - D_n)}{F_i}$ ratio of incremental nozzle thrust minus drag to ideal thrust

APPARATUS AND PROCEDURE

The material presented is drawn from a number of investigations involving a variety of jet-exit testing techniques. Data were obtained principally from strut-supported models at zero angle of attack using cold air or the decomposition products of hydrogen peroxide as the jet fluid. Some single nacelle axisymmetric boattailed bodies, some simplified twin-jet afterbody configurations, and a limited amount of data on complete aircraft configurations were considered. The methods of obtaining the various types of results are explained in the referenced reports. Inlet flow was not simulated during the powered model tests, but the effects of faired-over inlets on long duct fighter type models have generally been found to be small (ref. 4). Various kinds of nozzles have been employed, but these are well known from the literature and no details except as to type are included herein. Coefficients of thrust and drag are generally presented as incremental values since the objective is to indicate trends as variables are changed.

DISCUSSION

The discussion is divided into four sections: first, attempts to illustrate the magnitude of the aft-end drag problem for real aircraft configurations; then, some theoretical and empirical considerations of afterbody drag on simple bodies; followed by discussions of airframe installation effects on nozzle performance and, conversely, the effects of nozzle installation on aircraft performance.

Aft-End Drag of Twin-Engine Fighter Aircraft

Many military aircraft have twin engines buried in the rear of the fuselage. This combination can lead to relatively high drag for the afterbody portion of the aircraft. This results from the generally lower afterbody fineness ratio compared with the forebody

fineness ratio, the steep closure slopes required to fair in the nozzles, and the greater proportional wetted area of the empennage region. In addition, the rear portion of the aircraft with control surfaces, appendages, etc., is a region of high mutual interferences between surfaces immersed in a complex flow field.

The contribution of the afterbody relative to the total drag of some twin-jet aircraft configurations at subsonic speeds is illustrated in figure 1. Data are presented for zero lift. The research model had the wings fully swept back (fig. 2). The afterbodies of these models comprised about one-third of the model length but produced over 40 percent of the total configuration drag. Also shown on the bar graphs of figure 1 are the percent friction drag on the afterbodies and the amount of the jet-interference increment. The ratio of afterbody to total wetted area for the research model was 36 percent and for the fighter model was 32 percent. The jet-interference increment is defined as the afterbody drag difference between the powered model with jets at the operating pressure ratio and the jet pressure ratio corresponding to that for a model with flow-through-nacelles. The sum of the friction drag and the jet-effects drag accounts for 50 to 60 percent of the drag on the afterbodies. The remainder is due to interferences in the afterbody region and the pressure drag on the afterbody.

A similar comparison at a transonic Mach number of 1.2 is presented in figure 3. The data are for low angles of attack and the skin friction coefficients have been adjusted for full-scale Reynolds numbers for a Mach number of 1.2 at sea level (ref. 3). The research model is the same configuration as shown in figure 1, with the afterbody containing about 36 percent of the total wetted area. With the jets operating at a typical turbofan pressure ratio for a Mach number of 1.2, the afterbody drag of the research model was 41 percent of the total drag. Skin friction on the afterbody represents about 15 percent of the total drag; while the jet-interference drag is only 1 percent of the total. These two items account for about 40 percent of the afterbody drag, indicating that the interference and wave drag constitute a major portion of the afterbody drag at transonic speeds.

The afterbody of the development model (see fig. 4) comprised only one-fourth of the complete model length but had 39 percent of the total wetted area. The afterbody drag for similar operating conditions was 46 percent of the complete model drag. These results show that a large percentage of the total drag can occur on a relatively small portion of the afterbodies of twin-engine configurations at transonic speeds. For this model the skin friction drag of the afterbody was about 16 percent of the total drag and the jet-effects drag was about 8 percent of the total. This model had blow-in-door ejector nozzles, and drag on the blow-in-doors is charged to the propulsion system (ref. 2). In general, the jet-interference effect is a relatively low proportion of the total drag for the examples shown, which indicates that early estimates of the performance of these config-

urations could be obtained with flow through models with the proper aft end geometry. It should be noted, however, that accurate evaluation of the installed nozzle concept is dependent on powered model results.

Aft-End Flow Field Environment

An example of the static pressure distribution occurring around the nozzle of a twin-engine fighter aircraft model at subsonic speed and jet operating condition is shown in figure 5. Pressure coefficient is plotted versus peripheral angle for orifice rows near the airframe-nozzle interface (solid line) and an axial station at about the mid point of the nozzle (broken line). A large distortion of pressures around the nozzle caused by the proximity of aircraft surfaces can be observed. The variation of pressure distribution for the two axial stations on the nozzle is quite different, both as a result of the change in nozzle shape and contour of the aircraft surfaces. This illustrates the complex flow field existing in the nozzle region of twin-engine aircraft and points out the difficulty in attempting to estimate the pressure distribution in the terminus region of this type of vehicle.

A further complication arises because the afterbody is a region where the boundary layer is thick and subject to perturbations. The boundary layer is affected by both adverse and favorable pressure gradients, shocks may be embedded in the flow, and many afterbody regions have interfering surfaces which cause local channel flows. All these factors tend to distort boundary-layer profiles; an example obtained on the afterbody of a twin-engine fighter model is shown in figure 6. Similar distortions of boundary-layer shapes ahead of a nacelle nozzle under a wing have been presented in reference 7. Both nonuniform static pressure distributions around three-dimensional afterbody contours and complex viscous-flow shape factors occur in the afterbody/boattail environment. It is evident that isolated boattail analysis, either analytical or experimental, is not adequate to evaluate complex fighter-type aft-end drag performance.

Afterbody Drag of Idealized Bodies

Because of the complex three-dimensional viscous flow on afterbodies of aircraft configurations, some experimental and theoretical studies on simplified afterbodies have been conducted in order to illustrate the trends of the forces on aft-ends when systematic variation of different geometric parameters are examined. It should be noted that the simplified-body approach is exploratory in nature and the complete flow field of each new aircraft should be duplicated to obtain quantitative results.

Pressure distributions on boattailed afterbodies.- Several methods are available for computing the drag of axisymmetric bodies at subsonic speeds. Two examples of the calculation of pressure distribution over a boattailed body at a Mach number of 0.80 are

given in figure 7. The stream-tube curvature theory of reference 8 computes the jet plume shape; whereas, the Douglas-Neumann method (ref. 9) assumes a cylindrical exhaust plume with smoothing at the exit-plume interface. Both methods provide good agreement with experimental measurements on an afterbody from reference 10. This and calculations by other researchers have shown that for simplified axisymmetric bodies at subsonic speed theoretical methods are available which adequately predict boattail pressure distributions on afterbodies with unseparated flow.

Subsonic afterbody drag.- In order to illustrate the proportionate drag on the afterbody of an idealized truncated body of revolution at subsonic speeds, figure 8 has been prepared. A Sears-Haack body with a fineness ratio of 7 was selected for the calculation of pressure and friction drag using the methods of references 9 and 11. The effect of boundary layer on pressure drag has been accounted for by adding the boundary-layer displacement thickness to the body coordinates. The solutions were iterated until the displacement thickness and the pressure distributions converged. Computations were conducted for afterbodies truncated at various fractions of body length. A hyperbolic representation of the wake was used to model the jet plume shape. For comparison to an equivalent shape of an aircraft with engines located at the terminus of the afterbody, truncation at 90 percent of the body length was assumed (total drag coefficient, 0.141). If the afterbody consists of 30 percent of the truncated length, the afterbody drag of this portion of the body is about 28 percent (0.068 at 0.90x/L minus 0.029 at 0.63x/L) of the complete model drag. This example indicates that, although subsonic pressure drag exists on truncated afterbodies, the friction forces still dominate; consequently, the afterbody drag is roughly proportional to its length for an idealized case. For greater truncations the percentage of afterbody to total drag can increase since less pressure recovery is available over the rear closure portion of the body.

Transonic afterbody drag.- The amount of drag on the afterbody of an aircraft configuration at transonic speeds can be examined by referring to an area distribution and equivalent body truncation location of a typical fighter and applying these geometric constraints to an idealized body of revolution. The fineness ratio to the engine exit location of a twin-engine fighter was determined to be about 75 percent of the length of an equivalent closed body of revolution with a fineness ratio of 10. Using these values, the wave drag and skin friction drag of a series of Sears-Haack bodies have been determined for a Mach number of 1.2 (fig. 9). The Sears-Haack body was truncated at fractions of body length from 0.5 to 1.0. The wave drag was computed by the method of reference 12 and skin friction drag was calculated using the method of reference 13 for wind-tunnel conditions. The afterbody of this configuration consisted of about 23 percent of the airplane length (ℓ = 0.17x/L). The total drag coefficient of the truncated Sears-Haack body is about 0.142. The drag coefficient of the Sears-Haack body truncated at the split line is

about 0.100. The drag coefficient increment of 0.042 represents about 30 percent of the total drag on the assumed model length. It is apparent that at transonic speeds the afterbody drag of even idealized body shapes contributes a proportionally large share of the total drag.

From these examples of the drag on simple axisymmetric afterbodies, the total drag on the afterbody is roughly proportional to its length and wetted area at subsonic speeds and is proportionately greater at transonic speeds. The data presented previously on real aircraft aft-ends indicated a much larger percentage of the total drag appeared on these complex afterbodies. In addition to the increment due to skin friction on the empennage, mutual interference between afterbody-empennage-nozzle components can account for further increases in afterbody drag.

Jet Effects on Boattails and Bases

The theoretical examples of afterbody drag did not consider the possible influence of the jet efflux interference on the boattail region. Studies of jet-interference effects on isolated nozzles of various types have been conducted by many organizations during the last 25 years (ref. 14). Nozzle internal performance is generally well documented and can be predicted with a high degree of confidence. The isolated nozzle performance in a flowing airstream, however, includes the nozzle external forces consisting of viscous and pressure drag, as well as the internal efficiency. Jet operation can alter the performance of the nozzle to produce either favorable or unfavorable effects on nozzle drag. This is illustrated in figure 10, taken from reference 15, where two circular arc boattails having the same projected area are compared. The high-fineness-ratio boattail having attached flow shows favorable jet-interference effects at subsonic and transonic speeds. Large decreases in boattail drag due to a base-bleed effect occur going from the jet-off point to the initial unchoked jet-on pressure ratios. Further increases in jet-pressure ratio to above the choked flow value tend to aspirate the flow near the exit of the afterbody, causing a slight increase in drag. At higher pressure ratios the jet pluming tends to pressurize the rear of the boattail, resulting in reductions in boattail drag. In contrast, the low-fineness-ratio boattail from which the flow was separated near the exit indicates that the jet generally aspirates the separated region as pressure ratio was increased, causing the drag to become higher. Similar results have been obtained on boattails with bases (ref. 14). Large bases separating the external flow from the internal jet were aspirated by jet operation.

When bases exist on twin-jet afterbodies, the jets can also aspirate or pressurize the base depending on the nozzle-base combination. Figure 11, taken from reference 16, illustrates this tendency for several Mach numbers. The configuration represented is a twin-jet afterbody model with a flat base between two adjacent convergent nozzles. Jet

effects on pressures measured on the base between these close spaced exhaust nozzles are illustrated for the convergent flaps closed down (normal or dry power) and opened for maximum augmented conditions. The symbols indicate orifice locations on a slightly recessed afterbody base. At $M = 0.8$ considerable variation in the base pressure coefficient occurred, depending on location; this was also true at $M = 1.2$ for the dry-power configuration. For the usual operating pressure ratios at these Mach numbers $\left(p_{t,j}/p_\infty = 2.9 \text{ at } M = 0.8 \text{ and } p_{t,j}/p_\infty = 4.5 \text{ at } M = 1.2\right)$, drag exists at the base. At $M = 2.2$ the pressure is constant over the base, and a slightly favorable force can result at an operating pressure ratio of 11.0.

Airframe Installation Effects on Nozzle Performance

The preceding section has indicated the jet-interference effects that can occur with isolated boattailed bodies of revolution. The twin-engine afterbody problems will be addressed in the following discussion.

The prediction of the installed performance of engine nozzles in an airframe can become quite difficult when one realizes the wide variety of propulsion exhaust systems and aircraft designs that can be conceived. Because of the large number of variables involved, it was felt that, at least for exploratory research, simplicity of the equipment would enhance the reliability of the results. A typical simplified twin-jet afterbody model of the type used in many of the investigations is shown in the photograph of figure 12.

Clustered jet exits.- Figure 13 is an example of a simplified installation consisting of multiple engines in a closely spaced package. The isolated nacelle shown on the left had a convergent-divergent nozzle with a 5° boattail. The same nozzle configuration in a side-by-side cluster of four engines with circular arc interfairings between them is shown in the right photograph.

In figure 14, results from the clustered installation are compared with those for the isolated nozzle. The variation of nozzle performance (gross thrust minus nozzle drag ratioed to isentropic thrust) with Mach number is presented for a typical turbojet pressure ratio schedule. The upper solid line is the performance of the uninstalled isolated nacelle, the short dashed line shows the installed performance for the in-line cluster, and the long-short dash curve is for the staggered arrangement. The drag term includes only the pressure drag on the nozzles. The main installation performance penalty occurs at transonic speeds where a decrement of about 2 percent exists, compared with values for the isolated nozzle. Staggering the two inboard engines had a slight beneficial effect at supersonic speeds because of favorable interference from the outboard jet exhausts on the boattails of the inboard nozzles. The low level of performance for this fixed convergent-divergent nozzle is due to comparisons being made for no secondary flow in the ejector although it was designed for a corrected weight flow ratio of 0.07 (ref. 17).

Afterbody boattailing upstream of nozzles.- In the figure on clustered jets (fig. 14), the nozzles had cylindrical approach sections at the nozzle attachment point. A variable in the design of an aircraft afterbody is the boattail angle upstream of the nozzle station, as indicated on the left-hand sketch of figure 15. For these twin-engine afterbodies, maximum cross-sectional area and engine lateral spacing were held constant. The afterbodies incorporated nozzle approach angles of 3°, 6°, and 9°, and the nozzles were of the iris convergent type with throat sizes to simulate dry power, maximum augmentation, and maximum power with shroud extended. Data are presented for jet pressure ratios appropriate to the selected values of Mach number.

The nozzle performance parameter is an increment relative to the nozzle static thrust ratio F_j/F_i. The shaded regions in the sketches of figure 15 indicate the nozzle surfaces on which the external stream can exert drag or thrust. At $M = 0.8$, pressure recovery in the external airstream exerts a thrust on the nozzle surface which causes the nozzle performance to exceed the static value. This favorable pressure recovery becomes more pronounced as the boattail angle is increased. Similar trends of increased upstream boattailing decreasing nozzle drag at subsonic speeds have been found with isolated boattails (refs. 14 and 18). At transonic speeds, approach angle had little effect on performance. At $M = 2.0$, the nozzle is underexpanded and supersonic jet interference pressurizes the boattailed portion of the shroud, producing a small favorable performance increment at the lowest approach angle. Increasing the approach boattail angle to 9° causes drag on the shroud as a result of lowering the level of pressures.

Tail interference on nozzle performance.- The combined interference of both horizontal and vertical tails on the installed performance of convergent-divergent nozzles in a twin-engine afterbody is illustrated in figure 16. Data are presented for a model angle of attack of zero and all tail incidence angles were zero degrees. The plot shows the variation of nozzle performance increment (tails on minus tails off) with Mach number. With these nozzles in the dry-power setting, for which the nozzle boattail angle was 14°, the addition of tails to the basic configuration caused a loss in nozzle performance of as much as 4 percent at $M = 0.95$. This loss is due primarily to reduced pressures on the nozzle boattail caused simply by proximity of another aerodynamic body, in this case the tail surfaces. In maximum augmentation this nozzle was almost cylindrical, and addition of the tail surfaces causes slightly favorable interference.

Boom extensions on afterbody.- In many fighter-airplane designs the engines and exhaust nozzles are located near the extreme aft end of the airplane. This approach frequently leads to a short coupled configuration requiring large tail surfaces, for which the trim drag may be large. One approach toward obtaining a longer tail moment arm is to mount both horizontal and vertical tails on outboard booms which extend downstream of the nozzle.

Figure 17 shows variation with Mach number of the change in exhaust nozzle performance caused by adding outboard booms to the basic twin-engine afterbody, the increment being expressed as a fraction of ideal gross thrust. The first trial of this concept (left-hand sketch) was disappointing in that severe losses in nozzle performance were incurred with convergent-divergent (C-D) nozzles at dry-power setting, though in maximum augmentation (max. aug.) the loss was relatively small. The poor design feature in this case was the restricted channels between engines and booms. The right-hand sketch shows the configuration used in a subsequent investigation of an afterbody with shrouded iris convergent nozzles and booms essentially integral with the nozzles. For this configuration, addition of the booms generally improved performance; there was no channel between the booms and the airframe and nozzles.

Afterbody shaping effects on nozzle performance.- The effect of twin-engine installation environment on exhaust-nozzle performance is further illustrated in the bar chart of figure 18 for subsonic dry power and augmented power at Mach numbers of 1.2 and 2.2. The performance parameter is an increment based on the static performance. Convergent (CONV.), convergent-divergent (C-D), conical plug (PLUG), and blow-in-door (B-I-D) nozzles were investigated with two afterbodies which differed in nozzle environment. All nozzles had the same primary throat area for a given power setting. The afterbody designated "smooth" was more or less idealized with contours that faired well into the nozzle external surfaces and had no base between the nozzles. The afterbody labeled "protrusions" incorporated a fuselage extension between the nozzles and a streamlined extension outboard of each nozzle. These fuselage extensions allowed clearance for changes in nozzle geometry with power settings but were not in physical contact with the nozzles. Performance of the exhaust nozzles in combination with the afterbody with protrusions is indicated by the hatched bars, in combination with the smooth afterbody by the open bars (see fig. 18).

At subsonic speeds, the smooth afterbody permits pressure recovery to progress to the end of the nozzles, resulting in thrust on the nozzle boattails. The installed performance generally exceeds the static values. The effect of protrusions is to spoil the potential character of the external flow in the vicinity of the nozzles with a consequent loss of nozzle boattail thrust. At $M = 0.8$ the installation effect between these two afterbodies for the convergent and convergent-divergent nozzles makes a difference in nozzle performance of about 11 percent of the gross thrust. At transonic speeds, the external flow exerts a pressure drag on the nozzle outer surface and reduces nozzle performance with both afterbodies. At supersonic speeds, the smooth afterbody provides the better operating environment for the nozzles.

This nozzle performance data presented in figure 18 are not intended for use in nozzle selection but rather to show generally that all nozzle types are similarly affected

by operating environment and preservation of undisturbed external flow over the nozzle boattail leads to improved performance. Similar nozzles installed in different afterbody configurations may show another order of relative merit.

Effects of lateral spacing on nozzle performance.- In twin-engine installations the lateral distance between engines can vary for a number of reasons. Several investigations have been conducted to determine the importance of engine spacing on installed nozzle performance. Simple afterbodies without tail surfaces were used in these studies, and all configurations had the same maximum cross-sectional area and essentially the same area progression for close and wide spaced nozzles. Three types of nozzles were examined: shrouded convergent-flap nozzles (ref. 16), convergent-divergent (ref. 19), and twin conical plug nozzles (ref. 20). The same throat areas for dry power and maximum augmentation were used for the different types of nozzles. The results of the lateral spacing study are presented in figure 19. Spacing ratio s/d_n is the distance between engine center lines divided by the maximum diameter of each type of nozzle. At a Mach number of 0.80 only the convergent-divergent nozzle installed performance was affected by lateral spacing. The performance decrement for the close spaced nozzles is similar to results previously shown for clustered jet convergent-divergent nozzles. At supersonic speed the convergent-divergent nozzles had cylindrical shapes, and no effect of lateral spacing was observed. For the other nozzle types lateral spacing had no effect on the installed performance. Similar results were found in reference 21; therefore, it appears that the effect of lateral spacing on exhaust nozzle performance is not a major consideration in aerodynamically clean configurations of the types tested.

Nozzle Installation Effects on Airframe Performance

Effect of jet-exit axial location on afterbody drag.- Engine-exhaust system installations in a fuselage provide many options for axial and lateral locations. The axial position depends on a trade between propulsion system weight and aircraft balance and the influence of the jet exhaust on vehicle performance, stability, and induced structural loading (ref. 22). The problem of axial location of jet exits in an afterbody arrangement was given elementary treatment in a study (ref. 23), which is illustrated in the sketches of figure 20, for afterbodies of equal size and overall length. The circles indicate the jet exits located at the extreme aft end, the squares indicate the exits moved forward by one-half body width, and the diamonds indicate exits moved forward by one full body width upstream of the wedge apex.

The results show the variation with Mach number of afterbody drag coefficient (based on A_{max}) with the jets operating at values of pressure ratio appropriate to Mach number for a turbofan engine (see fig. 20). Because drag is measured on only the aft portion of a complete body, the absolute values are not pertinent; however, the differences

in afterbody drag coefficient are significant. The dashed curve shows calculated drag coefficient for an axisymmetric afterbody having the same axial distribution of cross-sectional area as the afterbody having extreme aft location of the exits. Actually, all the afterbodies have the same basic Haack-Adams shape when the jets are cylindrical. At subsonic speeds, the configuration with exits at the extreme aft end has the lowest level of drag, and the afterbody drag increases as length of the interfairing is increased. This order of excellence is maintained at speeds up to a Mach number of about 1.3. At higher supersonic speeds, favorable interference of the jet plume reduces the drag of all configurations, but afterbodies having extended interfairings are better adapted to derive benefit from this effect (ref. 24).

Engine lateral spacing effect on afterbody drag.- Results of a study of lateral spacing on afterbody drag are given in figure 21. Drag coefficients for configurations having three types of nozzles (refs. 16, 19, and 20) are shown at representative Mach numbers for typical turbofan jet pressure ratios. Each type of nozzle installation had approximately the same axial distribution of cross-sectional area and the same fineness ratio for the two lateral spacings. Afterbody drag generally increases with spacing ratio for all configurations at all Mach numbers (an exception is the convergent nozzles at dry power and $M = 0.80$). The different levels of drag coefficient reflect slight differences in afterbody local fairings and in the area distributions required to accommodate the various types of nozzles.

Afterbody-plus-nozzle drag.- The previous figures have illustrated effects on the afterbody alone as influenced by nozzle position. The total drag on the aft end of an aircraft is the combination of the afterbody and nozzle drags. The amount of drag on these components for a closely spaced twin-engine afterbody configuration with convergent-divergent nozzles is depicted in figure 22 (ref. 5). Both of the boattailed nozzles show thrust occurs on the nozzle surfaces. The dry-power nozzle which has the most negative nozzle drag interacts on the afterbody to produce the highest afterbody drag. Since the drag of the components are of opposite sign the combination of afterbody plus nozzle drag is less than that of the afterbody alone. Thus, the total aft-end drag does not presently appear to be predictable because of the mutual interactions of the nozzle and afterbody on each other with jets operating, in addition to the complex flow field on the back end.

Effect of booms on total afterbody drag.- Figure 23 indicates the drag penalties that may have to be paid for adding booms to a clean afterbody. The results shown are for the same configurations previously illustrated in figure 17. The incremental drag coefficient for afterbody plus nozzles is the difference between booms on and booms off. The long booms with dry-power nozzles again indicate the largest drag penalty, reflecting losses similar to those shown for the nozzles in figure 17. The addition of booms to the basic afterbody results in increases in the total afterbody drag for all configurations.

Interfairing shape influence on afterbody-plus-nozzle drag.- The shape of the interfairing between the engine nacelles can influence the drag of the afterbody, the nozzles, or combination of afterbody and nozzles, depending on the termination point of the interfairing relative to the nozzles (refs. 5 and 6). The effect of two types of interfairing shape on the drag of the afterbody, the nozzles, and the sum of afterbody and nozzles is given in figure 24. Although the vertical wedge-extended interfairing has the lowest afterbody drag, it also produces drag on the nozzles, which is predominant in this case, so that the total afterbody drag is highest for the extended interfairing at subsonic speeds. The elliptical horizontal-wedge interfairing induced cleaner flow at the nozzles, resulting in nozzle surface thrust and lower total afterbody drag.

Figure 25 presents results on varying the interfairing shape for a closely spaced twin-jet afterbody configuration which had a 3° approach boattail angle to the nozzles. A three-position iris nozzle was tested in combination with several afterbody interfairings. Three interfairing shapes which terminated at the afterbody-nozzle interface were studied: a circular arc, an elliptical, and a blunt (flat base) configuration. In addition, an extended interfairing which was a continuation of the blunt configuration was utilized, and this interfairing terminated downstream of the longest nozzle in a small base. The variation of afterbody-plus-nozzle drag coefficient with Mach number for a typical jet-pressure-ratio schedule is given in figure 25. The upper-left plot shows data for the dry-power iris convergent nozzle. The lower-left data points are for the augmented iris configuration. The open symbols represent data for the augmented iris nozzles at transonic speeds; the solid symbols represent the augmented shrouded nozzle with elliptical and extended interfairings. The elliptical interfairing provides the lowest drag for the unshrouded nozzles, as shown by the dashed lines. The difference in afterbody-plus-nozzle drag between the blunt and elliptical interfairings for dry power represents an increase in drag coefficient of about 40 percent. For the augmented iris, the difference in drag coefficient for the same two interfairings is about 30 percent. At transonic speeds, small differences exist for the various interfairings. The shrouded augmented iris nozzle, which had less boattailing, was tested at supersonic speeds. An opposite trend is noted for the extended interfairing at these speeds as it now has the lowest drag. This trend has been observed previously (refs. 23 and 24) where a pluming jet can pressurize aft sloping surfaces, but extended interfairings generally have a detrimental effect on performance at subsonic speeds.

CONCLUDING REMARKS

The aft-ends of twin-engine fighter aircraft operate in a complex flow-field region which can cause the afterbody drag to become a high percentage of the overall drag. A review of exploratory studies of simplified afterbody-nozzle combinations has pointed out

many of the variables affecting the interferences between the exhaust system and the airframe. Experimental data presented have shown that aerodynamic refinement of the exhaust nozzle installation is of primary importance. Obstruction or disturbance of the potential nature of the external flow by airframe components in proximity to the exhaust nozzles generally leads to increased drag of the nozzle boattail and to degraded performance of the aircraft. The aft-end drag of real aircraft afterbodies was shown to be considerably higher than the afterbody drag calculated for simple idealized bodies. In twin-engine aircraft with engines mounted in the aft fuselage, lateral spacing of the engines does not appear to be a major design consideration. For aircraft having missions primarily at subsonic speeds, best performance was obtained with exhaust nozzles forming the downstream terminus, and moderately large approach boattail angles may be used without adverse effects on overall performance. For best performance of a supersonic aircraft, nozzle approach boattail angle should be kept to a small value, and a downstream extension of the fuselage between the nozzles may be advantageous.

Each of the components and design features that have been examined contribute an individual interference on the airframe-nozzle installation. Obviously, real aircraft designs will incorporate many of these arrangements in combination and will be subject to additional variables, such as deflection of aircraft surfaces and jet, protuberances, and attitude effects, all of which will make the back-end flow field even more complex. Jet interference acts predominantly on the nozzles, but the influence of the exhaust interference also extends forward onto the afterbody. Therefore, detailed simulation of the complete aircraft model and internal flows is required to provide the proper environment in the wind tunnel for prediction of installed nozzle performance and afterbody drag.

Langley Research Center,
National Aeronautics and Space Administration,
Hampton, Va., February 14, 1974.

REFERENCES

1. Nichols, Mark R.: Aerodynamics of Airframe-Engine Integration of Supersonic Aircraft. NASA TN D-3390, 1966.

2. Corson, Blake, W., Jr.; and Schmeer, James W.: Summary of Research on Jet-Exit Installations. NASA TM X-1273, 1966.

3. Runckel, Jack F.: Jet-Exit and Airframe Interference Studies on Twin-Engine-Fuselage Aircraft Installations. NASA TM X-1274, 1966.

4. Re, Richard J.; Wilmoth, Richard G.; and Runckel, Jack F.: Investigation of Effects of Afterbody Closure and Jet Interference on the Drag of a Twin-Engine Tactical Fighter. NASA TM X-1382, 1967.

5. Lee, Edwin E., Jr.; and Runckel, Jack F.: Performance of Closely Spaced Twin-Jet Afterbodies With Different Inboard-Outboard Fairing and Nozzle Shapes. NASA TM X-2329, 1971.

6. Glasgow, E. R.; and Santman, D. M.: Aft-End Design Criteria and Performance Prediction Methods Applicable to Air Superiority Fighters Having Twin Buried Engines and Dual Nozzles. AIAA Paper No. 72-1111, Nov.-Dec. 1972.

7. Head, Verlon L.: Flight Investigation of an Underwing Nacelle Installation of Three Variable-Flap Ejector Nozzles. NASA TM X-2478, 1972.

8. Keith, J. S.; Ferguson, D. R.; Merkle, C. L.; Heck, P. H.; and Lahti, D. J.: Analytical Method for Predicting the Pressure Distribution About a Nacelle at Transonic Speeds. NASA CR-2217, 1973.

9. Hess, J. L.; and Smith, A. M. O.: Calculation of Potential Flow About Arbitrary Bodies. Progress in Aeronautical Sciences, Vol. 8, D. Kuchemann, ed., Pergamon Press, Ltd., c.1967, pp. 1-138.

10. Compton, William B., III; and Runckel, Jack F.: Jet Effects on the Boattail Axial Force of Conical Afterbodies at Subsonic and Transonic Speeds. NASA TM X-1960, 1970.

11. Anon.: Users Manual for the External Drag and Internal Nozzle Performance Deck (Deck XI) – Supersonic Flow Analysis (Applicable to Deck VI). PWA-3465, Suppl. F, Pt. I (Contract No. AF33(615)-3128), Pratt & Whitney Aircraft, Sept. 1, 1968.

12. Harris, Roy V., Jr.: An Analysis and Correlation of Aircraft Wave Drag. NASA TM X-947, 1964.

13. Peterson, John B., Jr.: A Comparison of Experimental and Theoretical Results for Compressible Turbulent-Boundary-Layer Skin Friction With Zero Pressure Gradient. NASA TN D-1795, 1963.

14. Henry, Beverly Z., Jr.; and Cahn, Maurice S.: Additional Results of an Investigation at Transonic Speeds to Determine the Effects of a Heated Propulsive Jet on the Drag Characteristics of a Series of Related Afterbodies. NACA RM L56G12, 1956.

15. Reubush, David E.; and Runckel, Jack F.: Effect of Fineness Ratio on the Boattail Drag of Circular-Arc Afterbodies Having Closure Ratios of 0.50 With Jet Exhaust at Mach Numbers up to 1.30. NASA TN D-7192, 1973.

16. Maiden, Donald L.; and Runckel, Jack F.: Effect of Nozzle Lateral Spacing on Afterbody Drag and Performance of Twin-Jet Afterbody Models With Convergent Nozzles at Mach Numbers up to 2.2. NASA TM X-2099, 1970.

17. Kirkham, Frank S.; Lee, Edwin E., Jr.; and Lauer, Rodney F., Jr.: Afterbody Drag of Several Clustered Jet-Exit Configurations at Transonic Speeds. NASA TM X-1216, 1966.

18. Bergman, Dave: Implementing the Design of Airplane Engine Exhaust Systems. AIAA Paper No. 72-1112, Nov.-Dec. 1972.

19. Pendergraft, Odis C., Jr.; and Schmeer, James W.: Effect of Nozzle Lateral Spacing on Afterbody Drag and Performance of Twin-Jet Afterbody Models With Convergent-Divergent Nozzles at Mach Numbers up to 2.2. NASA TM X-2601, 1972.

20. Berrier, Bobby L.: Effect of Nozzle Lateral Spacing on Afterbody Drag and Performance of Twin-Jet Afterbody Models With Cone Plug Nozzles at Mach Numbers up to 2.20. NASA TM X-2632, 1972.

21. Mercer, Charles E.; and Berrier, Bobby L.: Effect of Afterbody Shape, Nozzle Type, and Engine Lateral Spacing on the Installed Performance of a Twin-Jet Afterbody Model. NASA TM X-1855, 1969.

22. Lee, Edwin E., Jr.; Foss, Willard E., Jr.; and Runckel, Jack F.: Jet Effects on the Base, Afterbody and Tail Regions of a Twin-Engine Airplane Model With High and Low Horizontal-Tail Locations. NASA TM X-2, 1959.

23. Berrier, Bobby Lee; and Wood, Frederick H., Jr.: Effect of Jet Velocity and Axial Location of Nozzle Exit on the Performance of a Twin-Jet Afterbody Model at Mach Numbers up to 2.2. NASA TN D-5393, 1969.

24. Pitts, William C.; and Wiggins, Lyle E.: Axial-Force Reduction By Interference Between Jet and Neighboring Afterbody. NASA TN D-332, 1960.

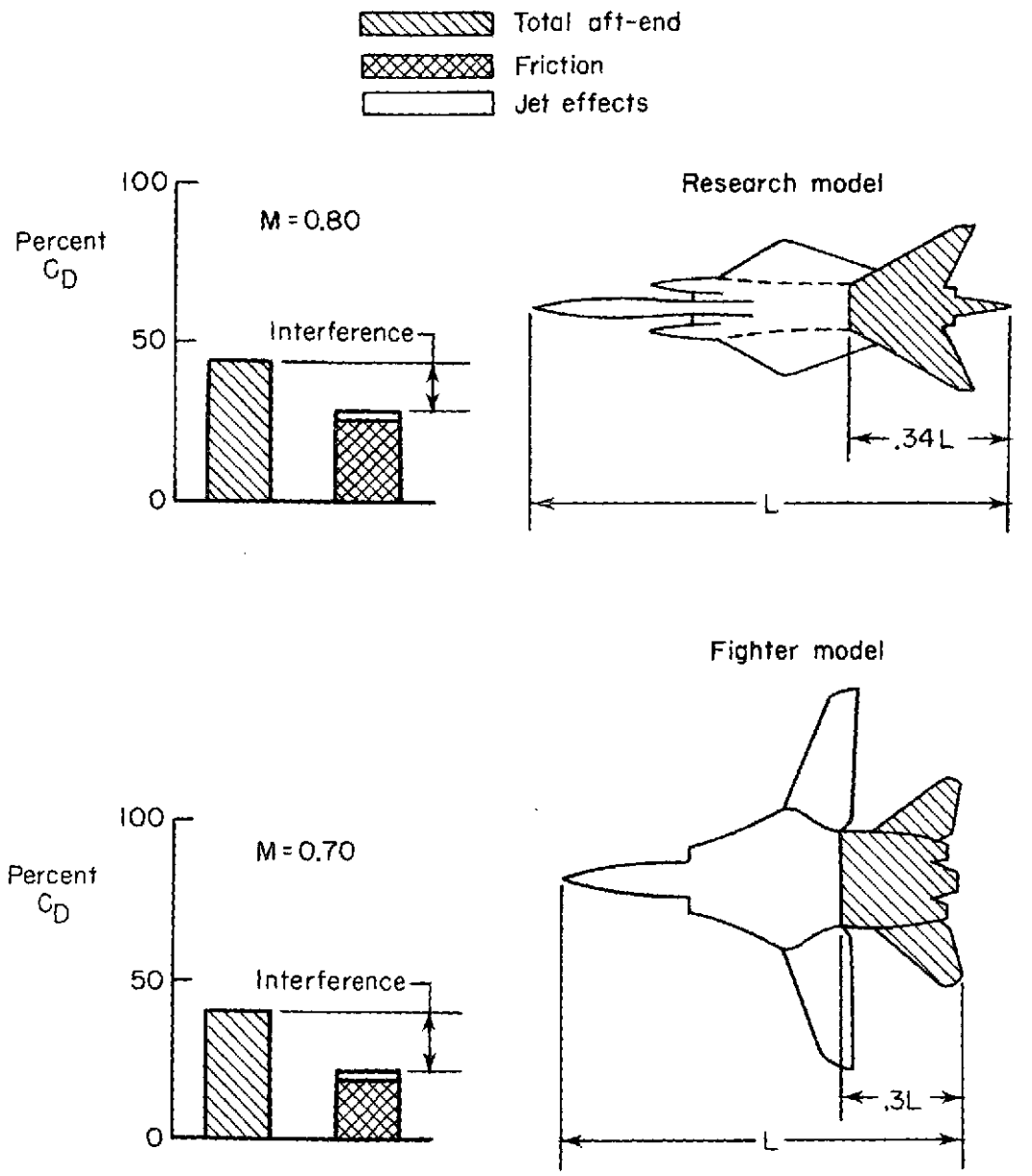

Figure 1.- Aft-end drag at subsonic speeds for lift coefficient of zero.

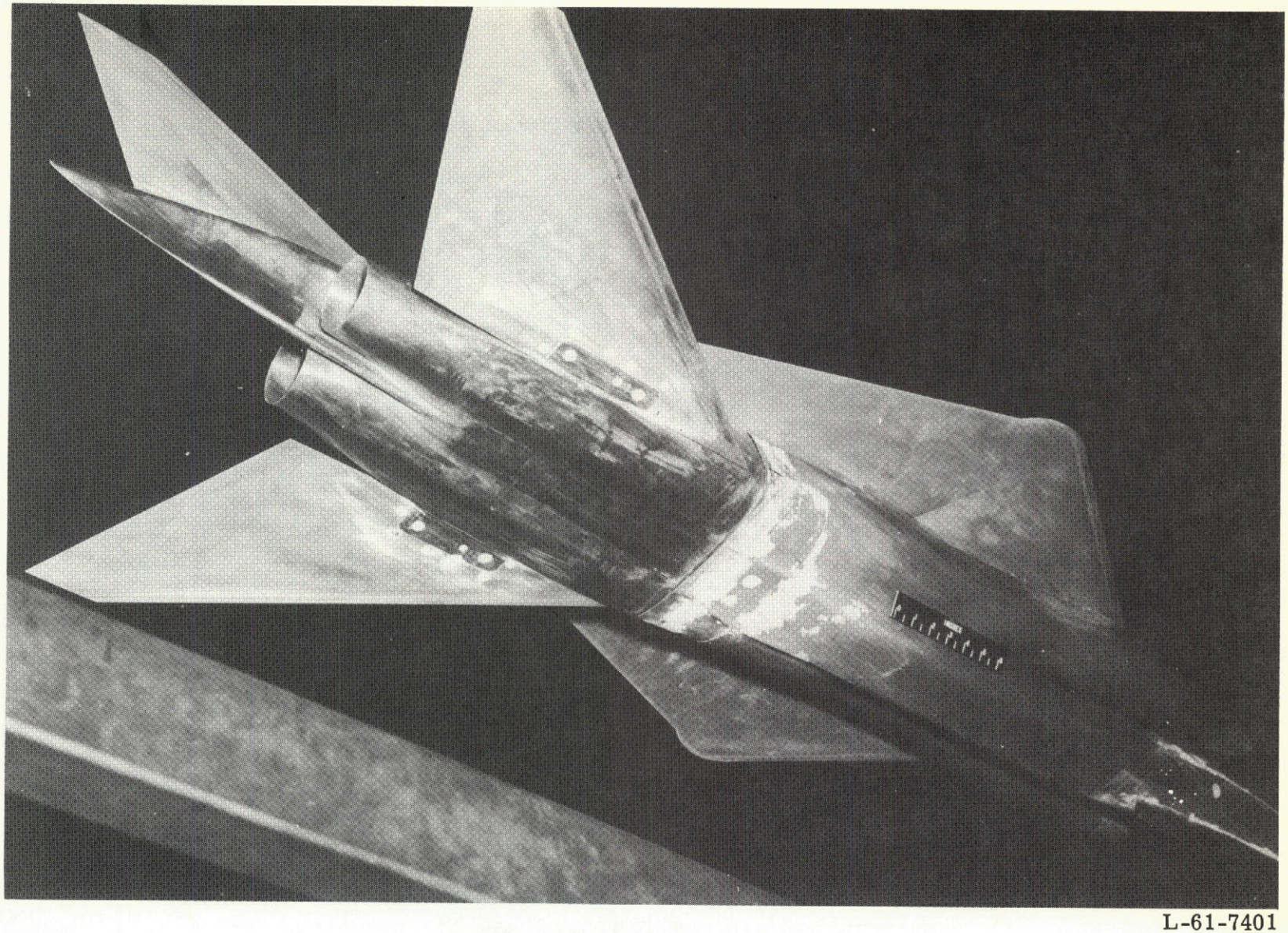

L-61-7401

Figure 2.- Research model.

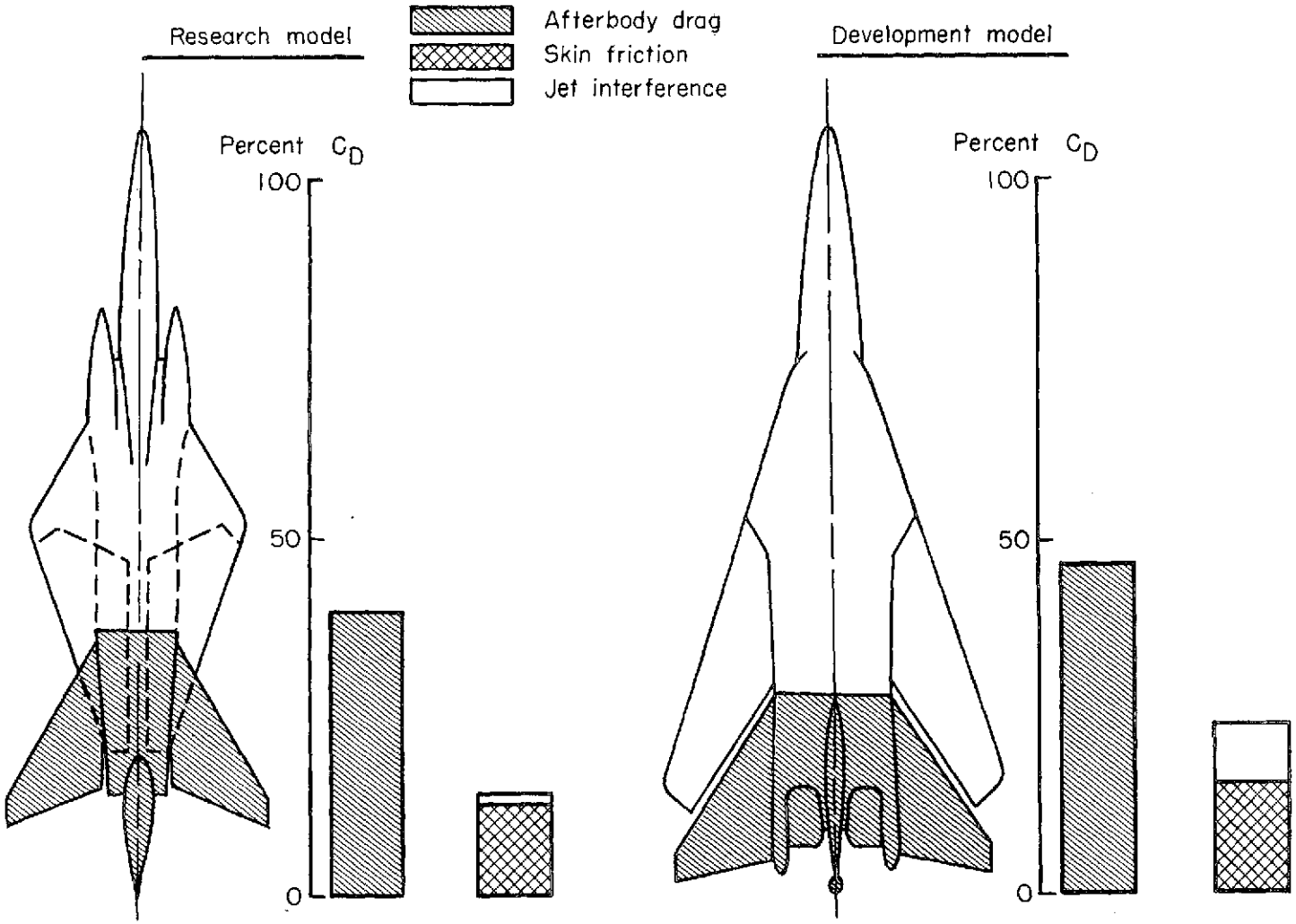

Figure 3.- Comparison of total and aft-end drag; M = 1.2 at sea level.

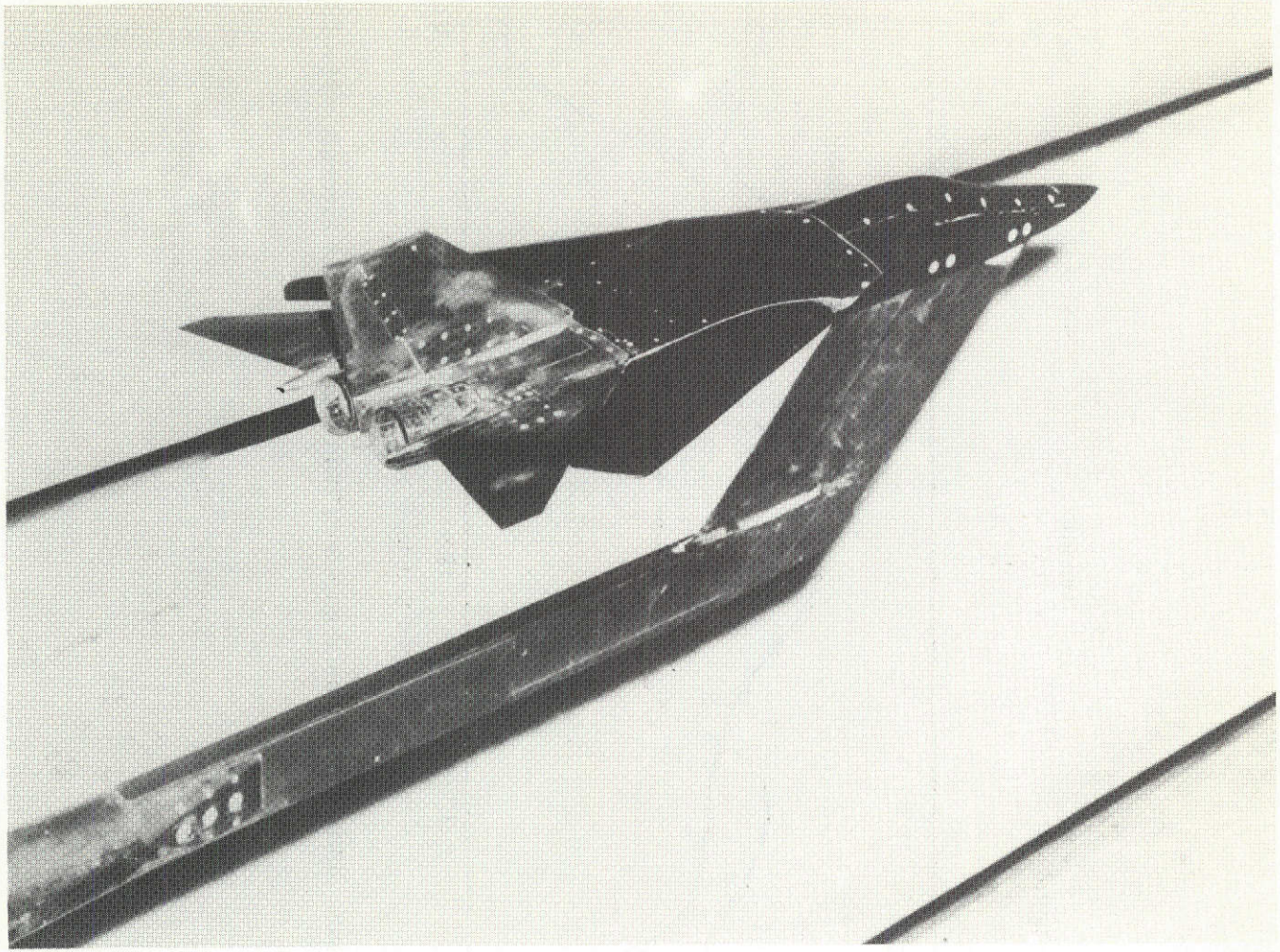

L-64-7574

Figure 4.- Development propulsion model.

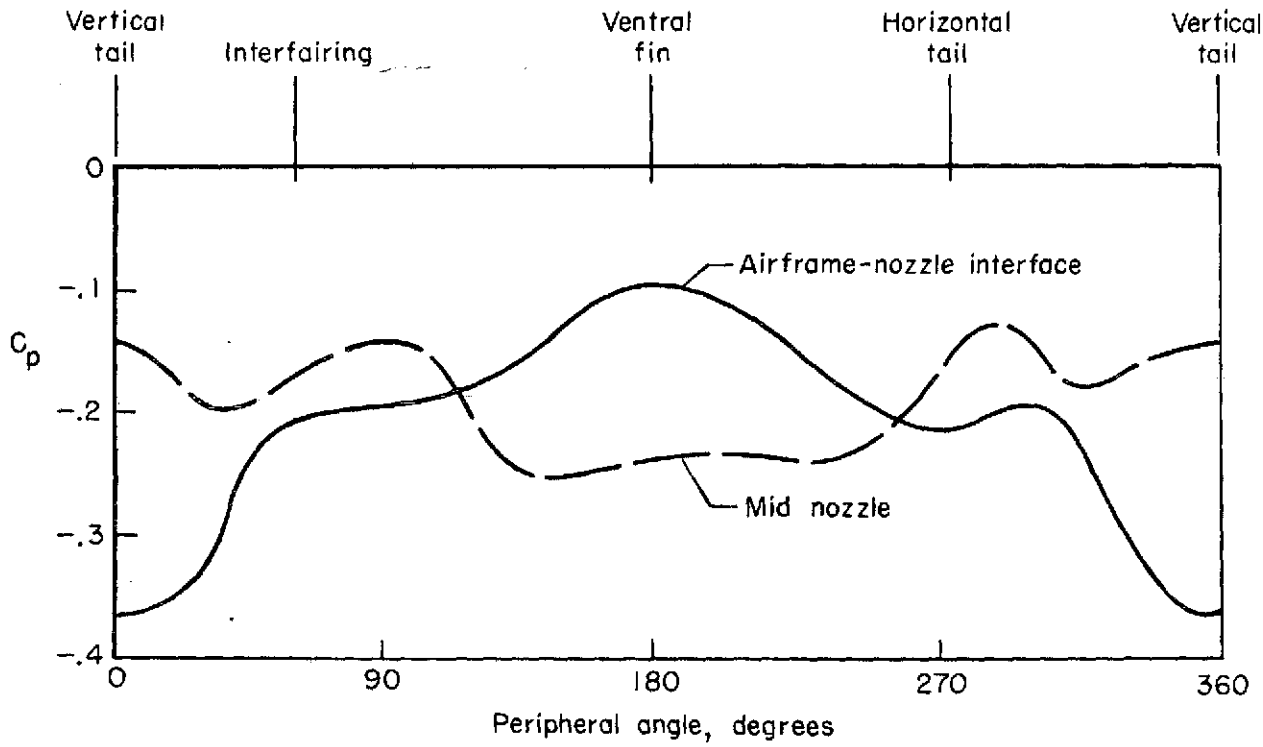

Figure 5.- Pressure distribution around nozzle of twin-engine fighter aircraft; M = 0.70.

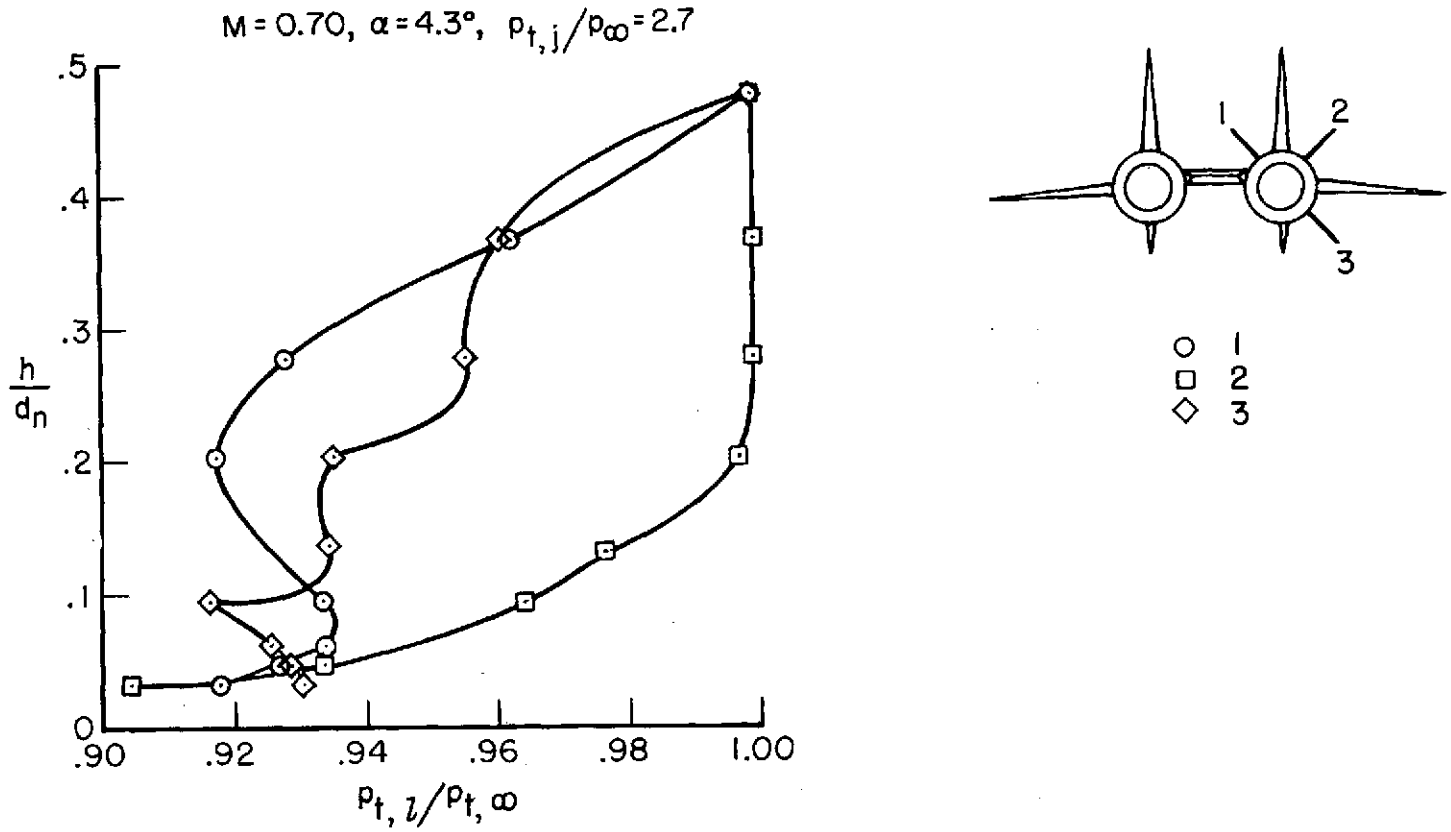

Figure 6.- Boundary-layer profiles at afterbody-nozzle interface of a twin-jet fighter model.

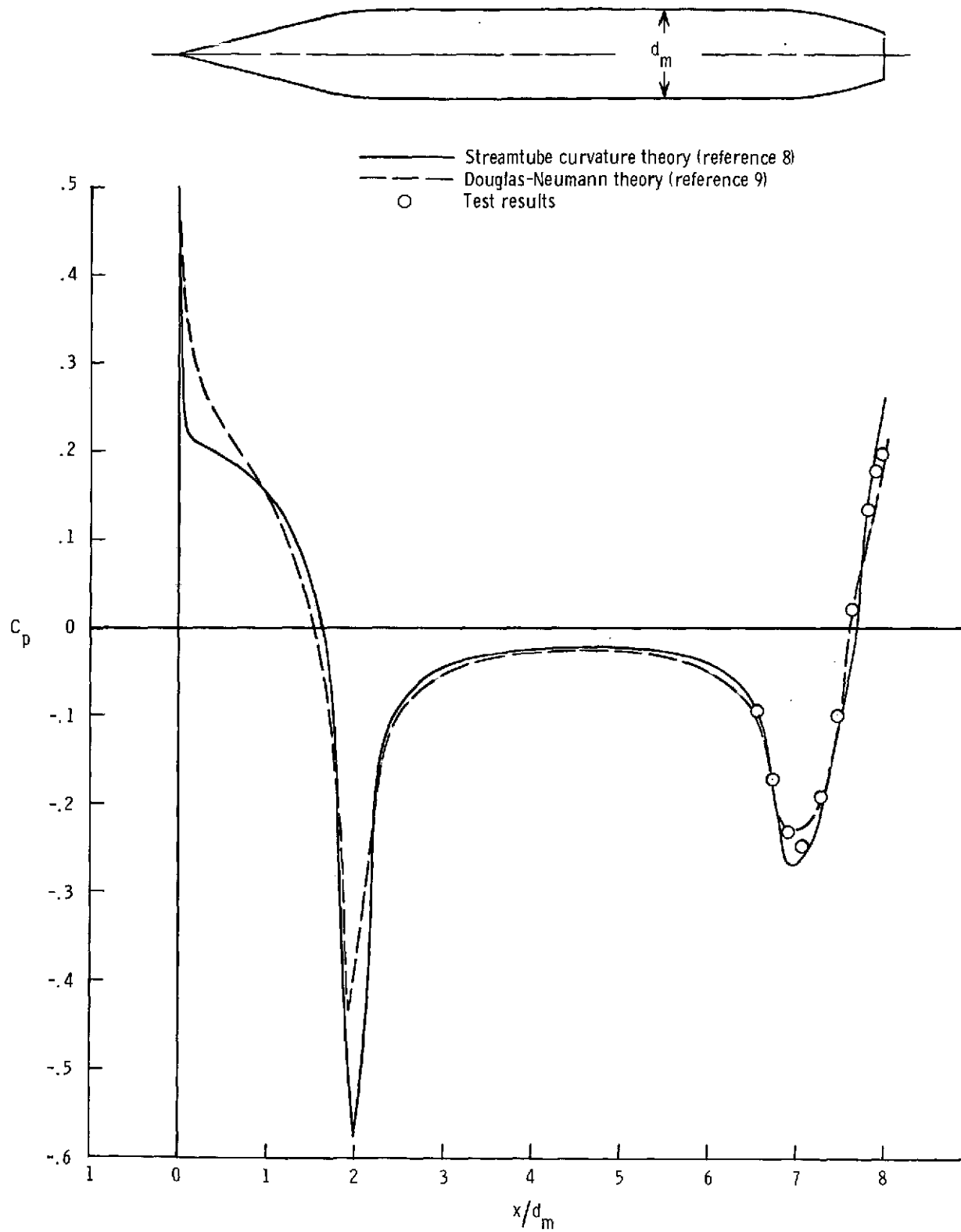

Figure 7.- Theoretical and measured pressure distributions; M = 0.80; $p_{t,j}/p_\infty = 2$. (Viscous corrections applied.)

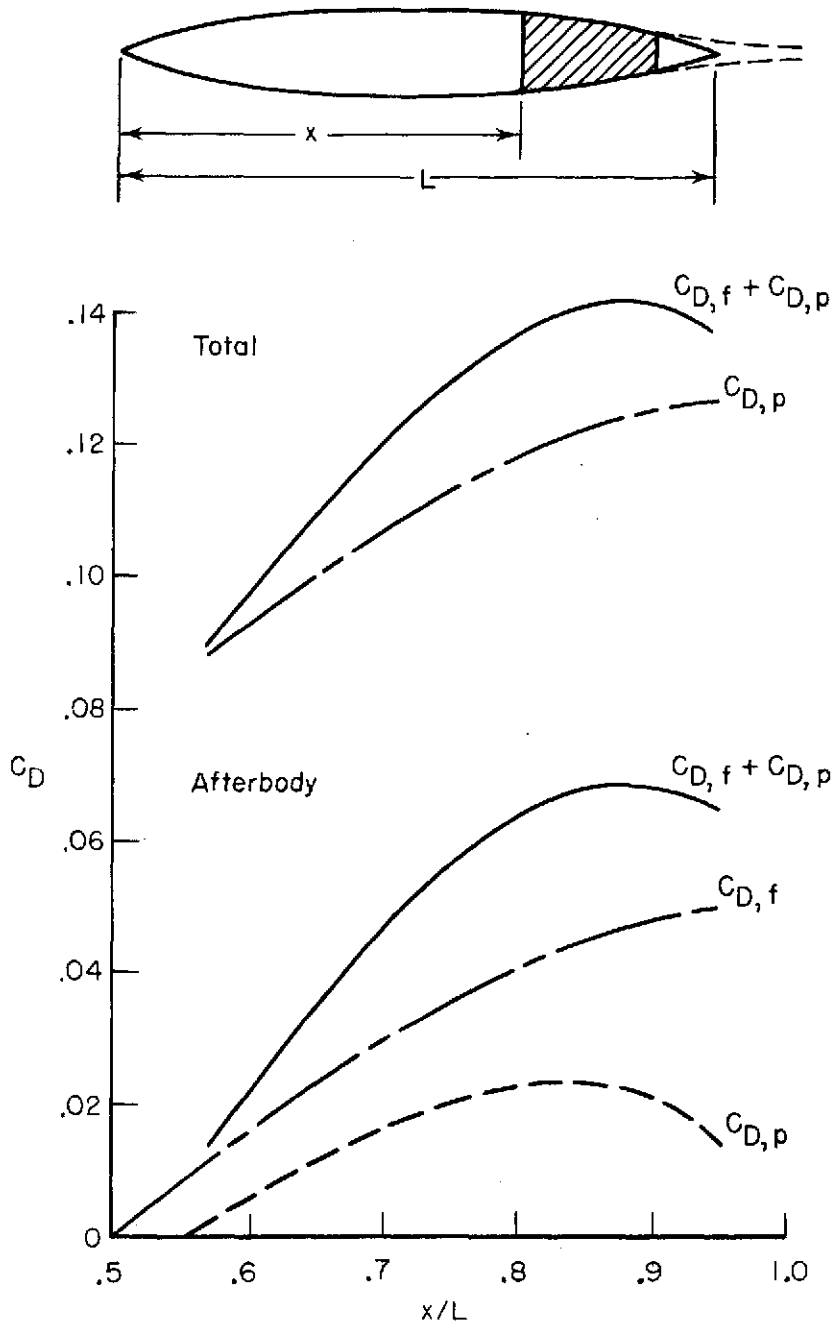

Figure 8.- Effect of truncation on drag of a boattailed body at M = 0.60.

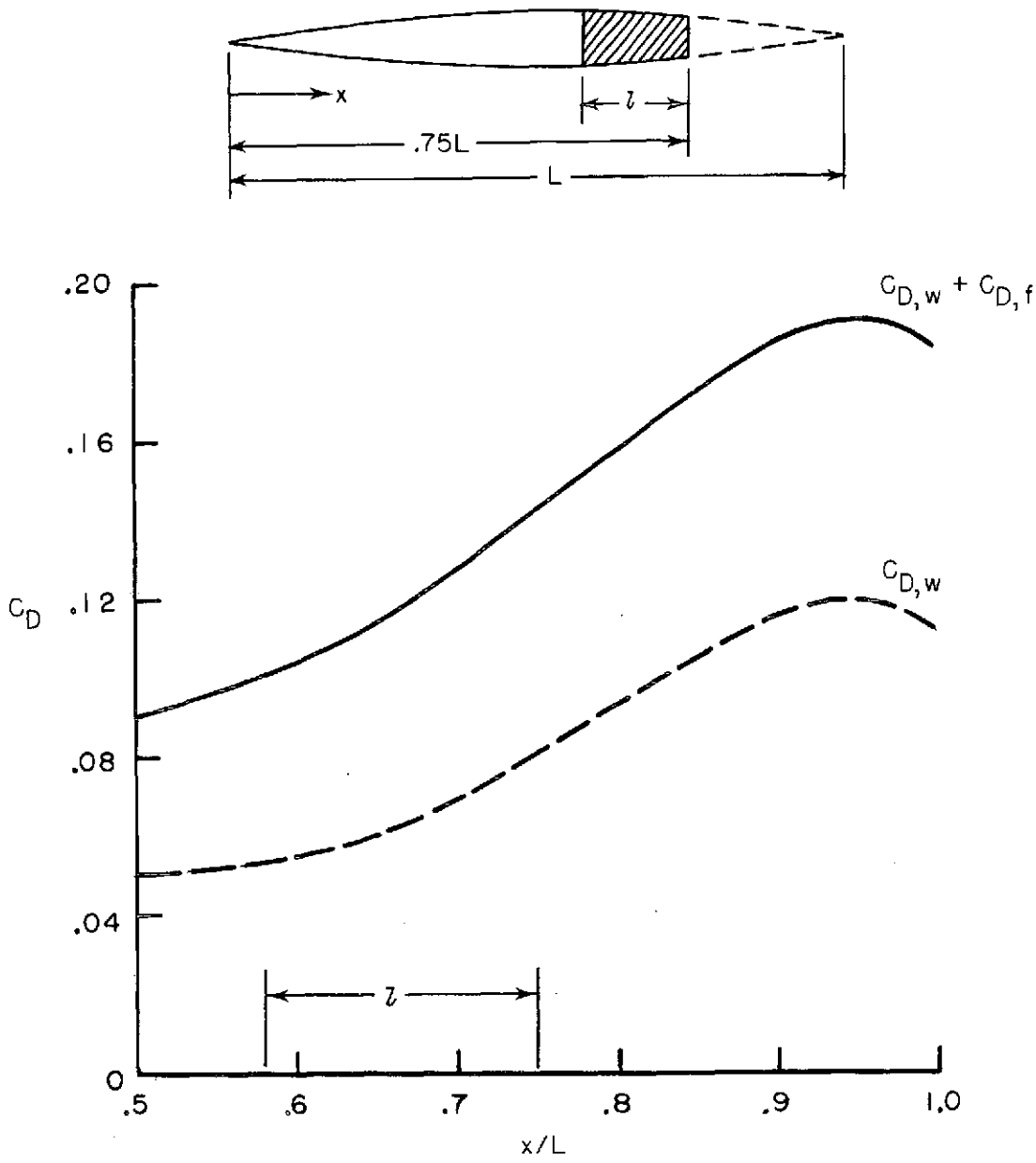

Figure 9.- Effect of truncation on drag of a boattailed body at M = 1.2.

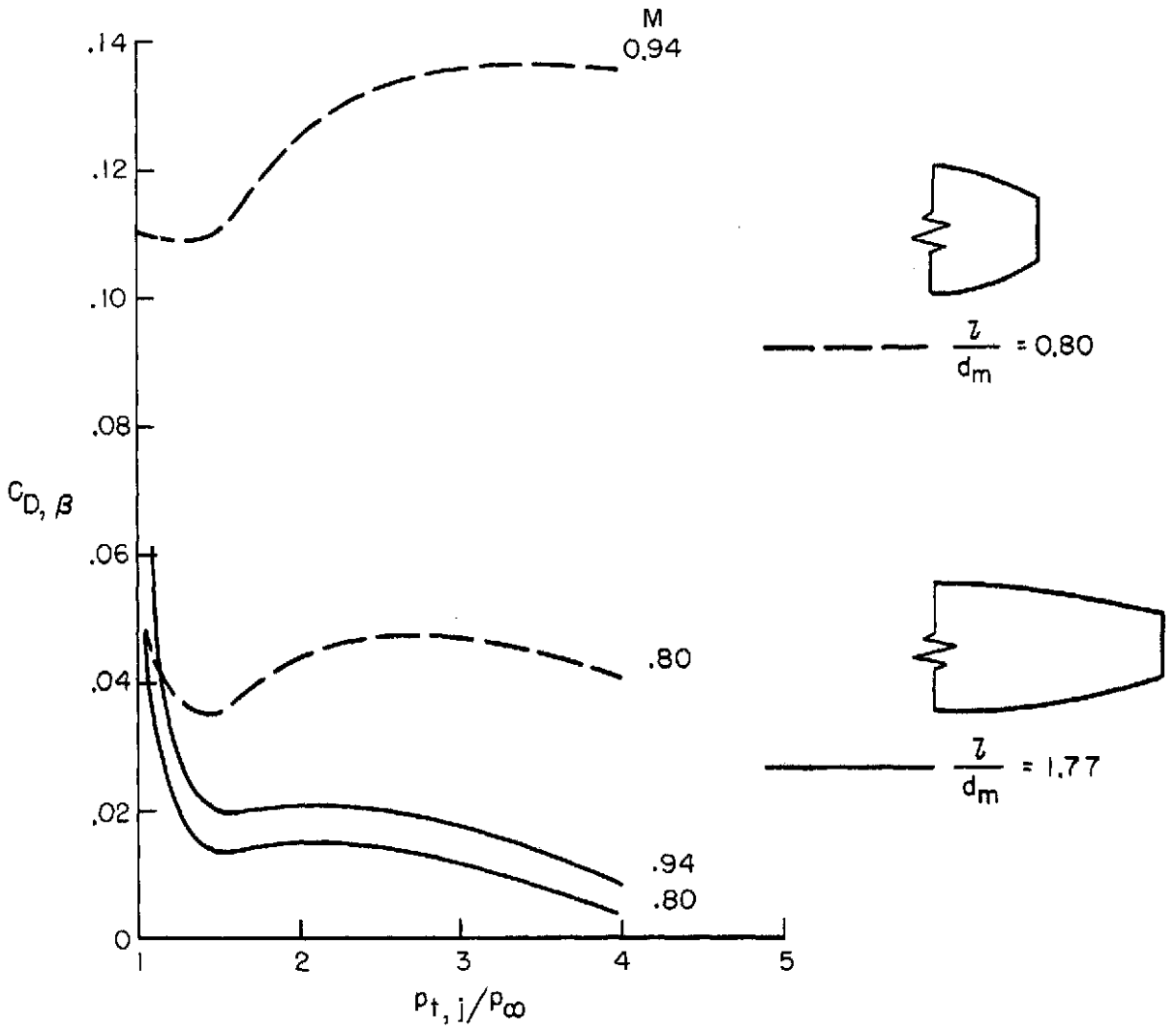

Figure 10.- Jet effects on different fineness ratio boattails; $d_e/d_m = 0.5$.

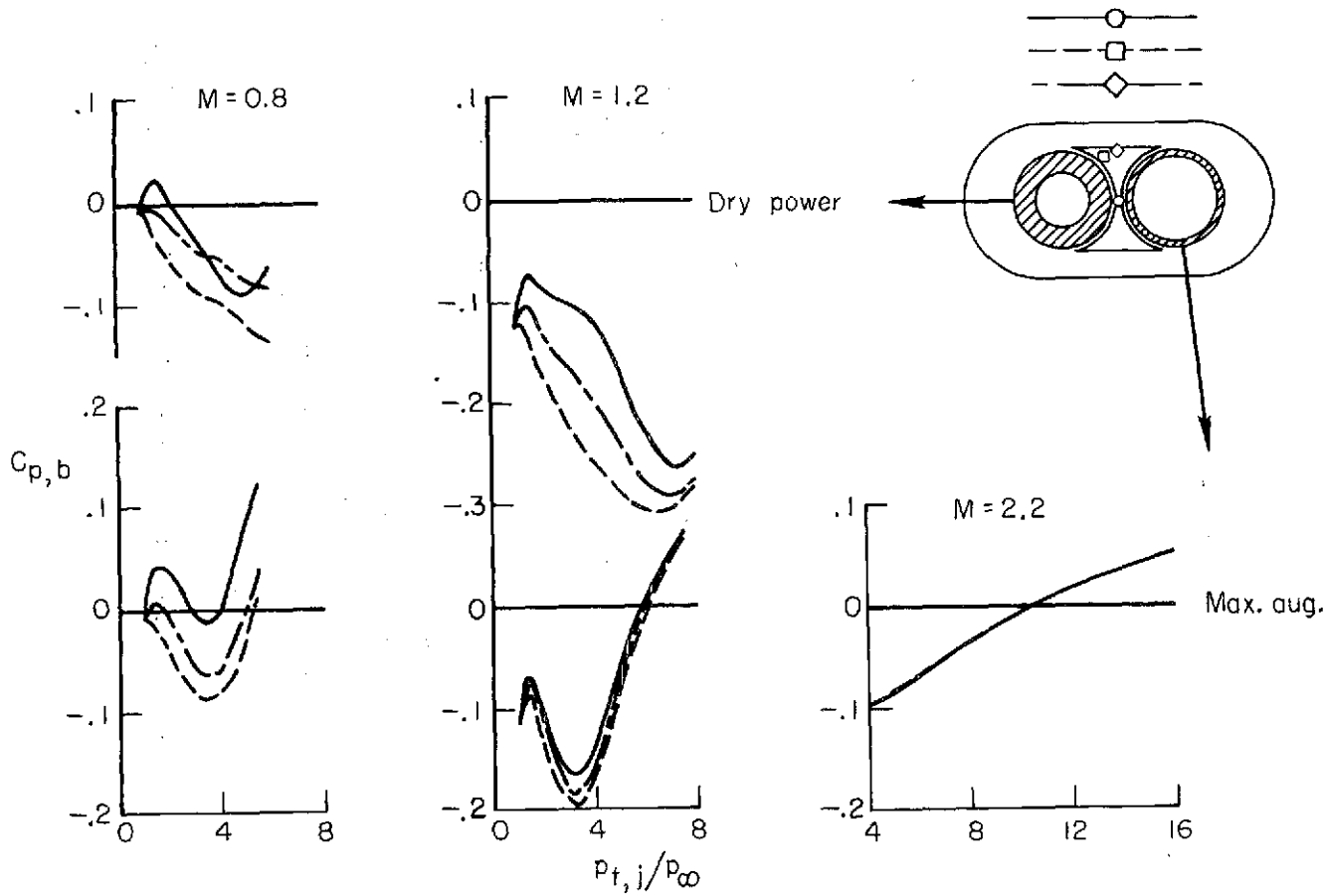

Figure 11.- Jet effects on afterbody base pressure coefficients.

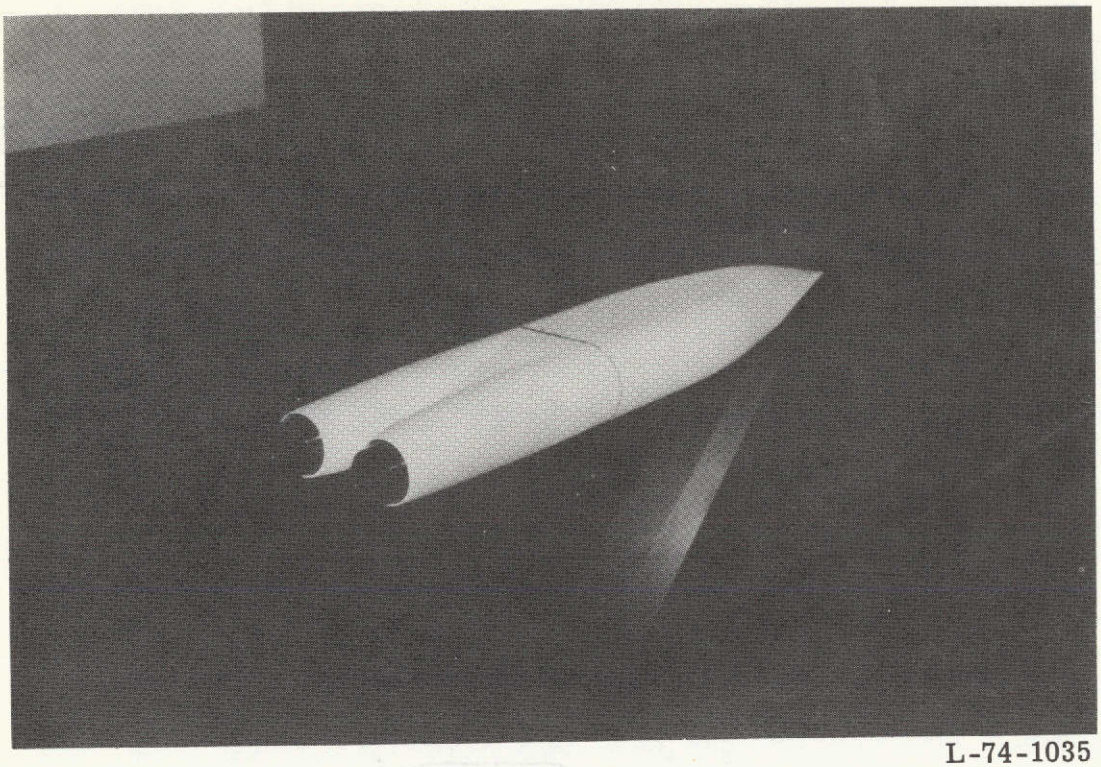

L-74-1035

Figure 12.- Twin-engine afterbody-nozzle model.

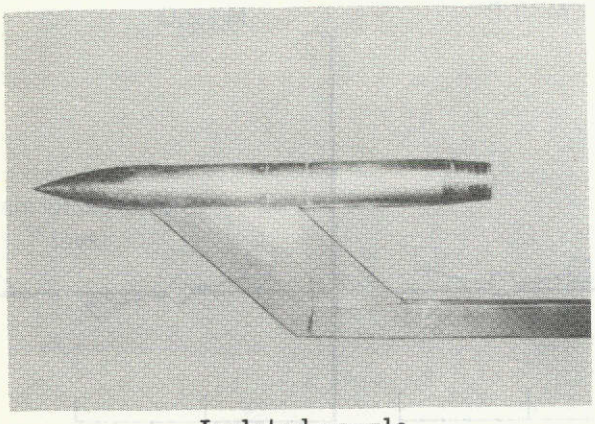

Isolated nozzle

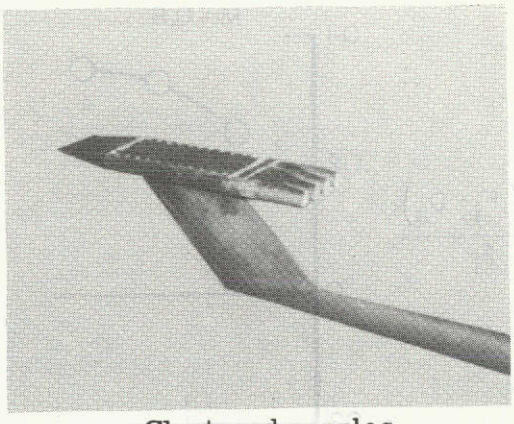

Clustered nozzles

L-74-1036

Figure 13.- Isolated and clustered jet installations.

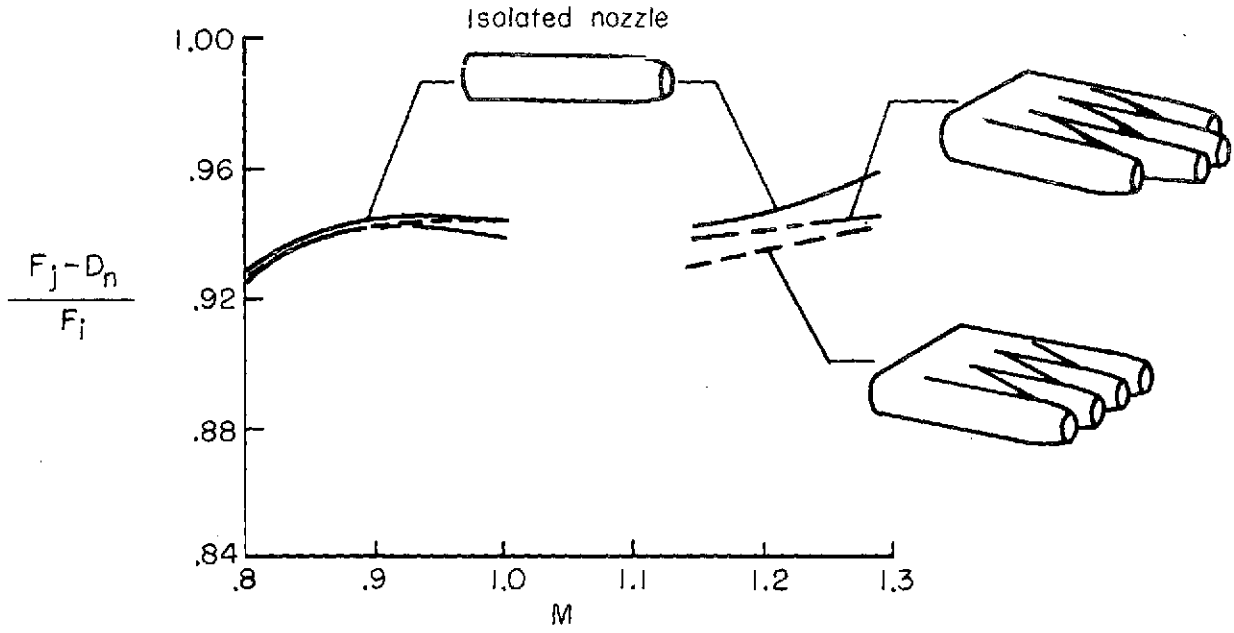

Figure 14.- Installed nozzle performance of clustered jet exits.

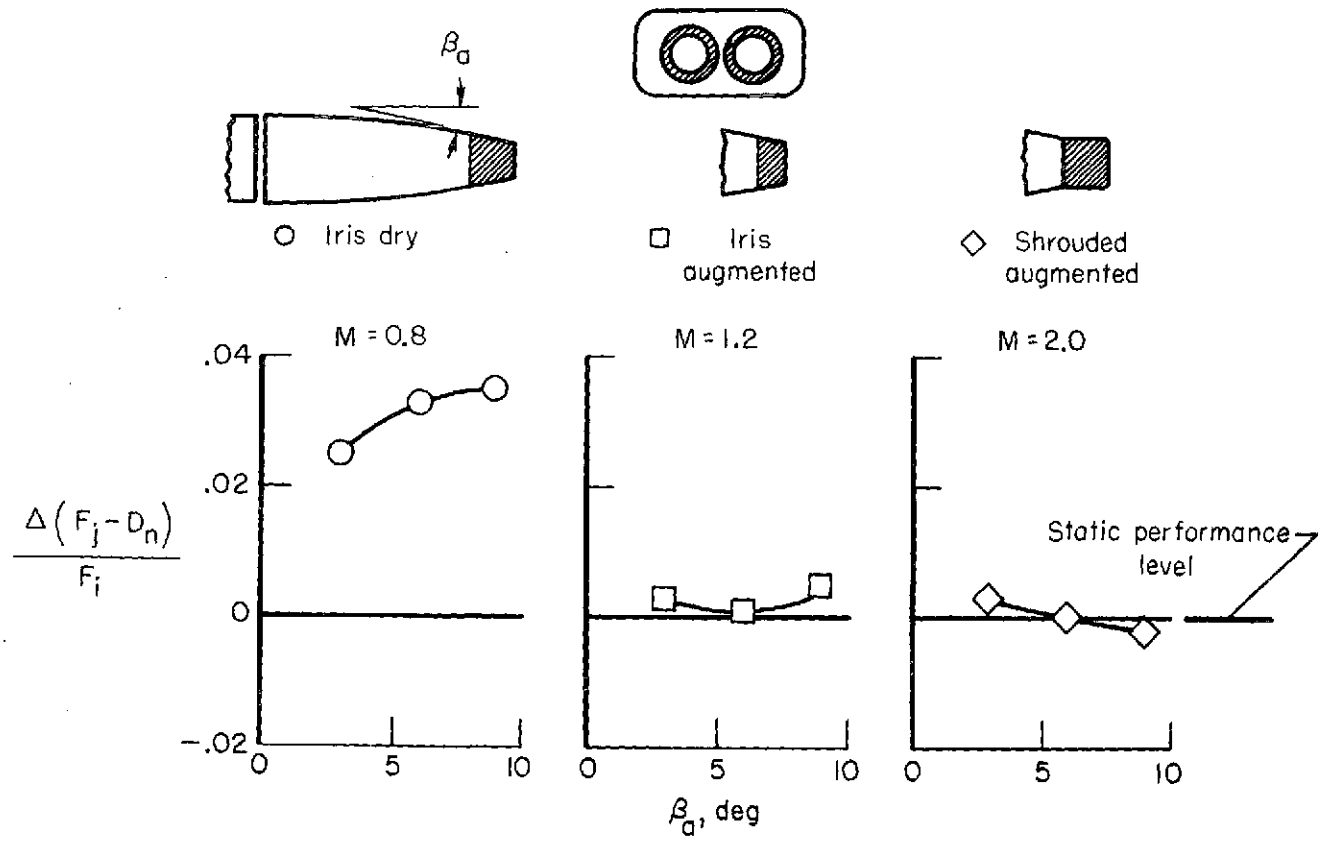

Figure 15.- Effect of afterbody approach angle on nozzle performance.

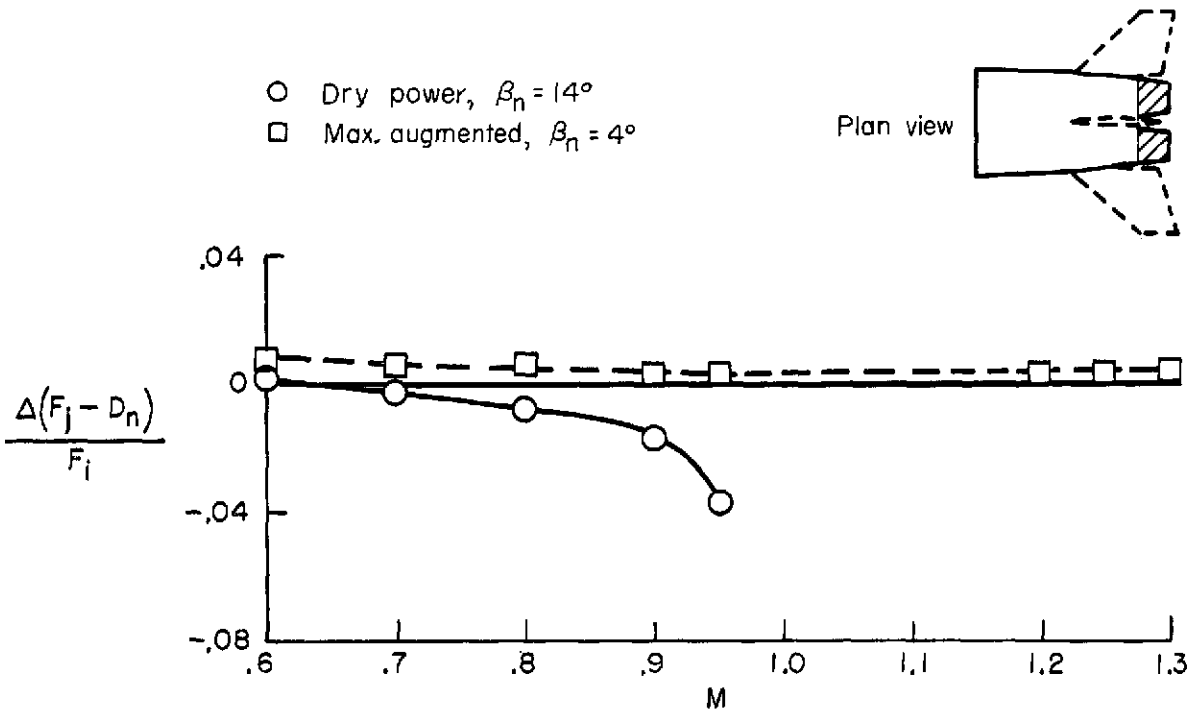

Figure 16.- Tail interference on nozzle performance.

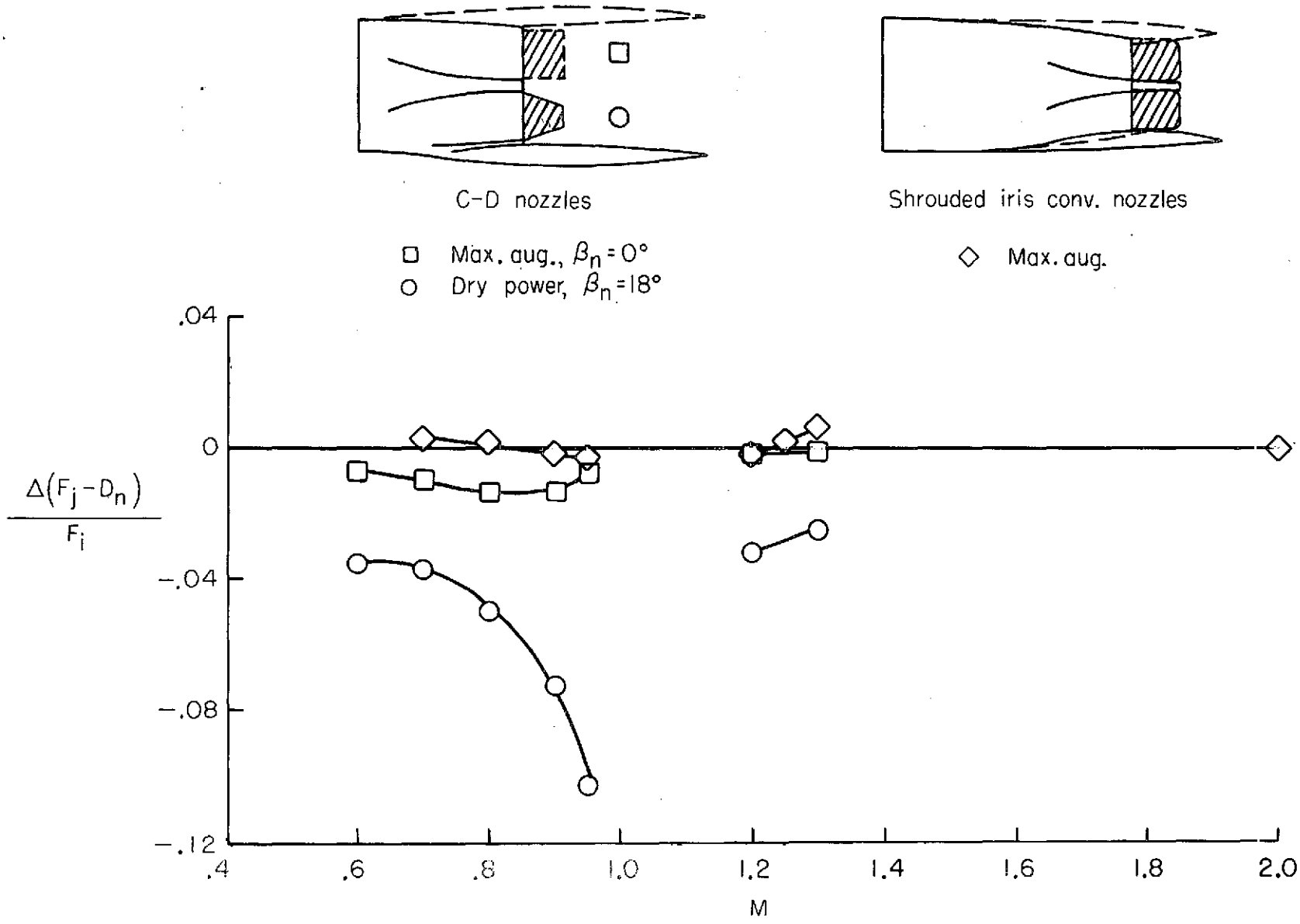

Figure 17.- Effect of addition of twin booms on nozzle performance.

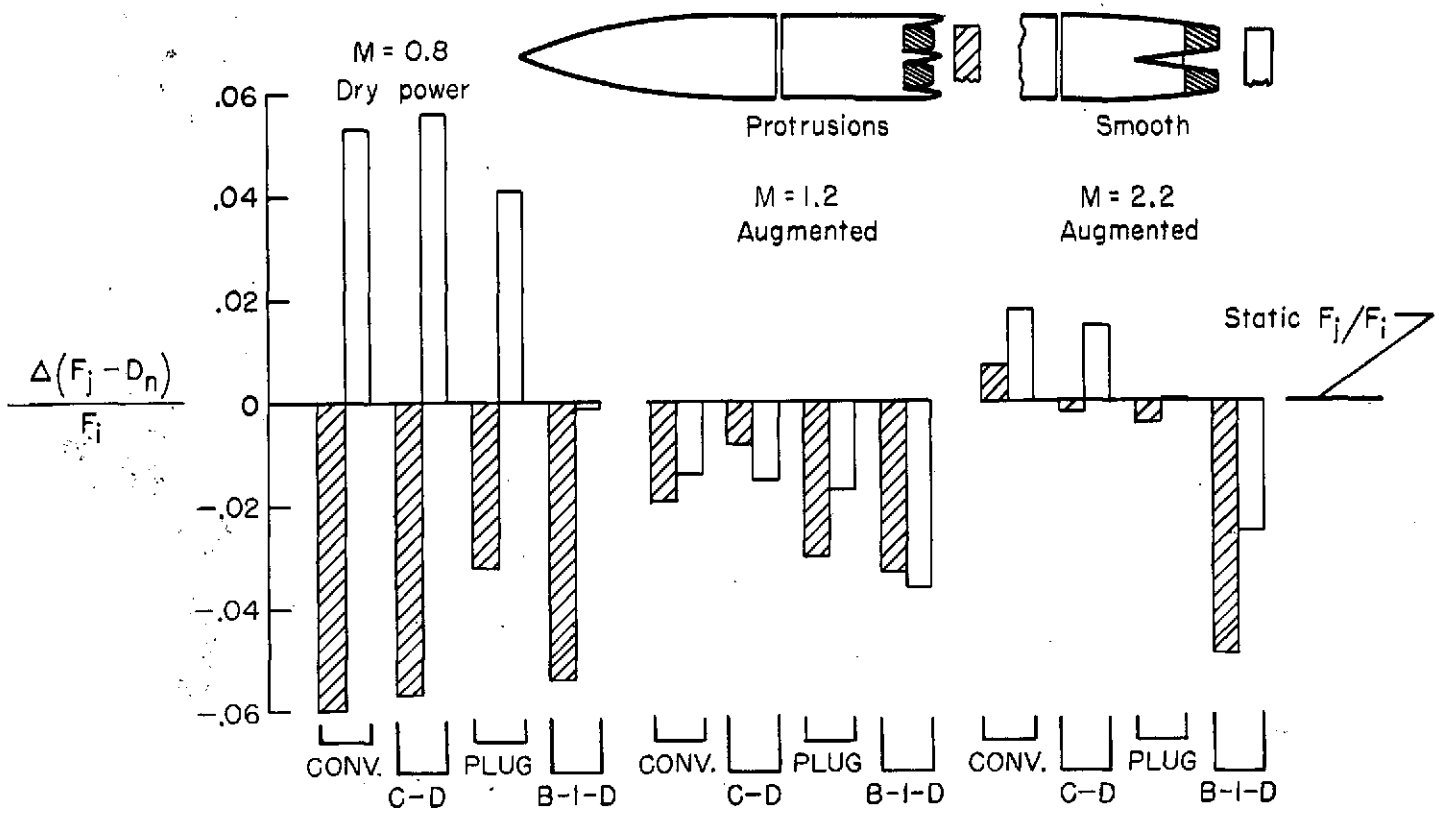

Figure 18.- Afterbody shaping effects on nozzle performance.

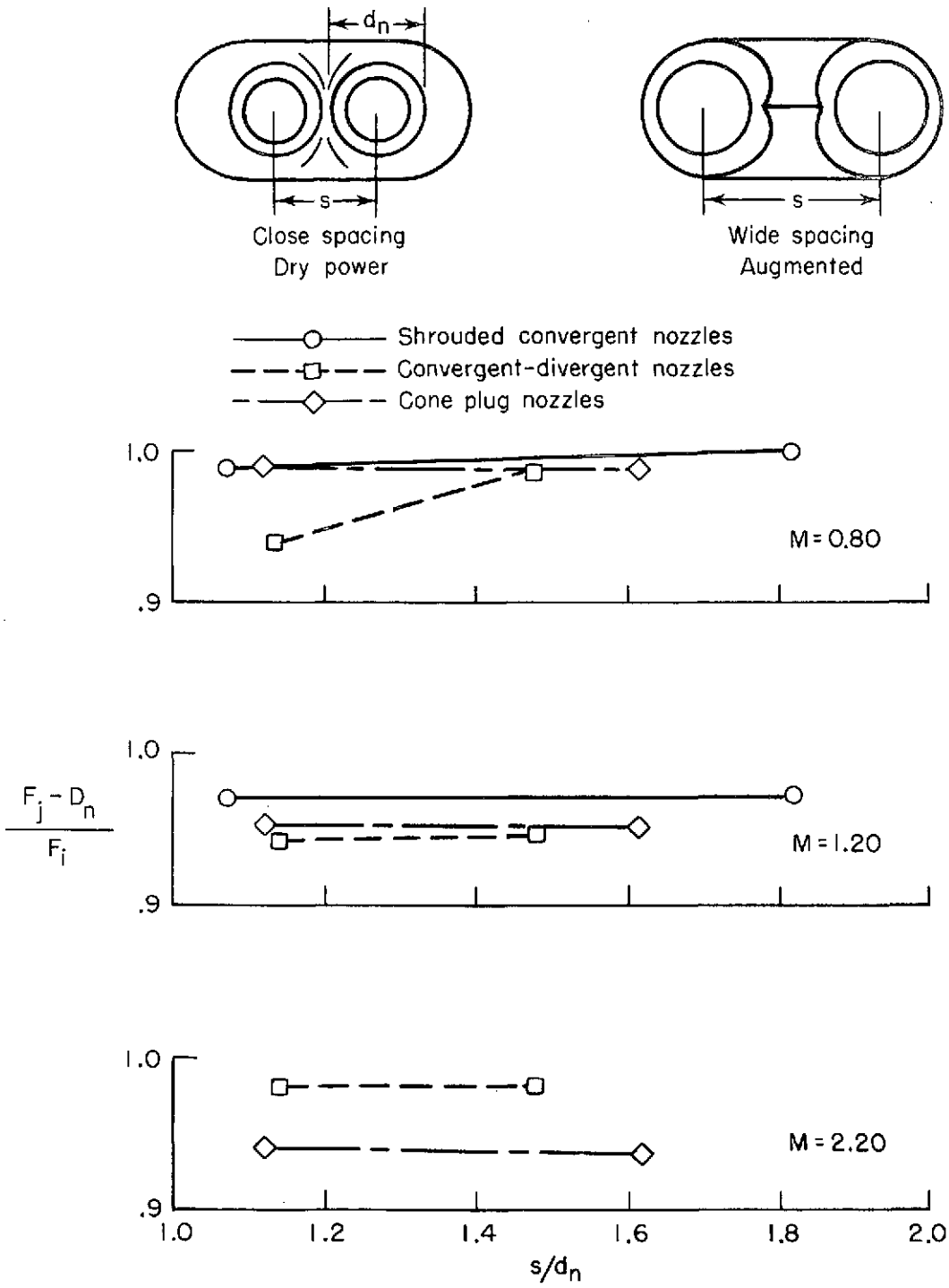

Figure 19.- Effect of lateral spacing on nozzle performance.

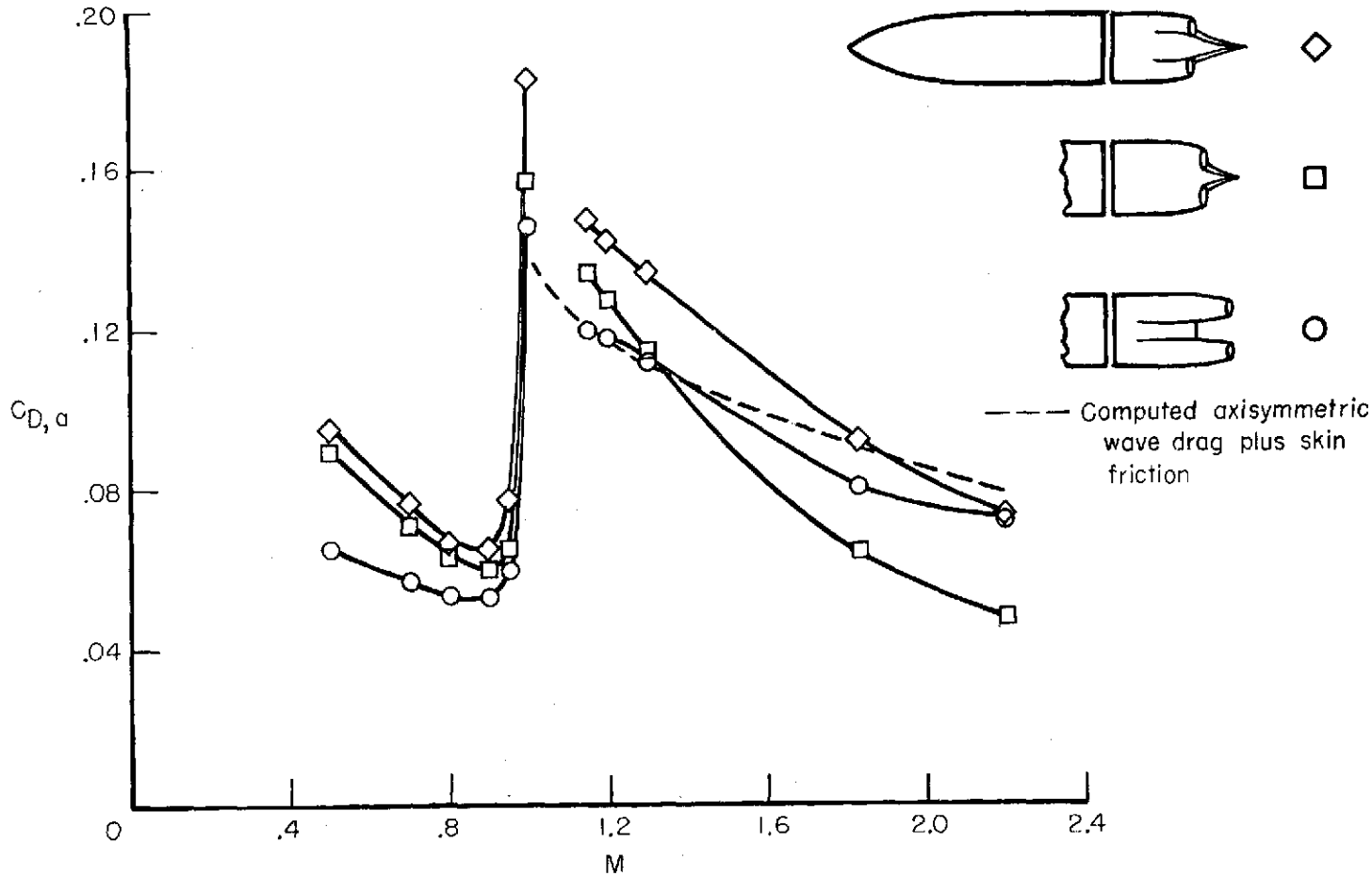

Figure 20.- Jet-exit axial location effect on afterbody drag. Pressure ratio schedule for turbofan.

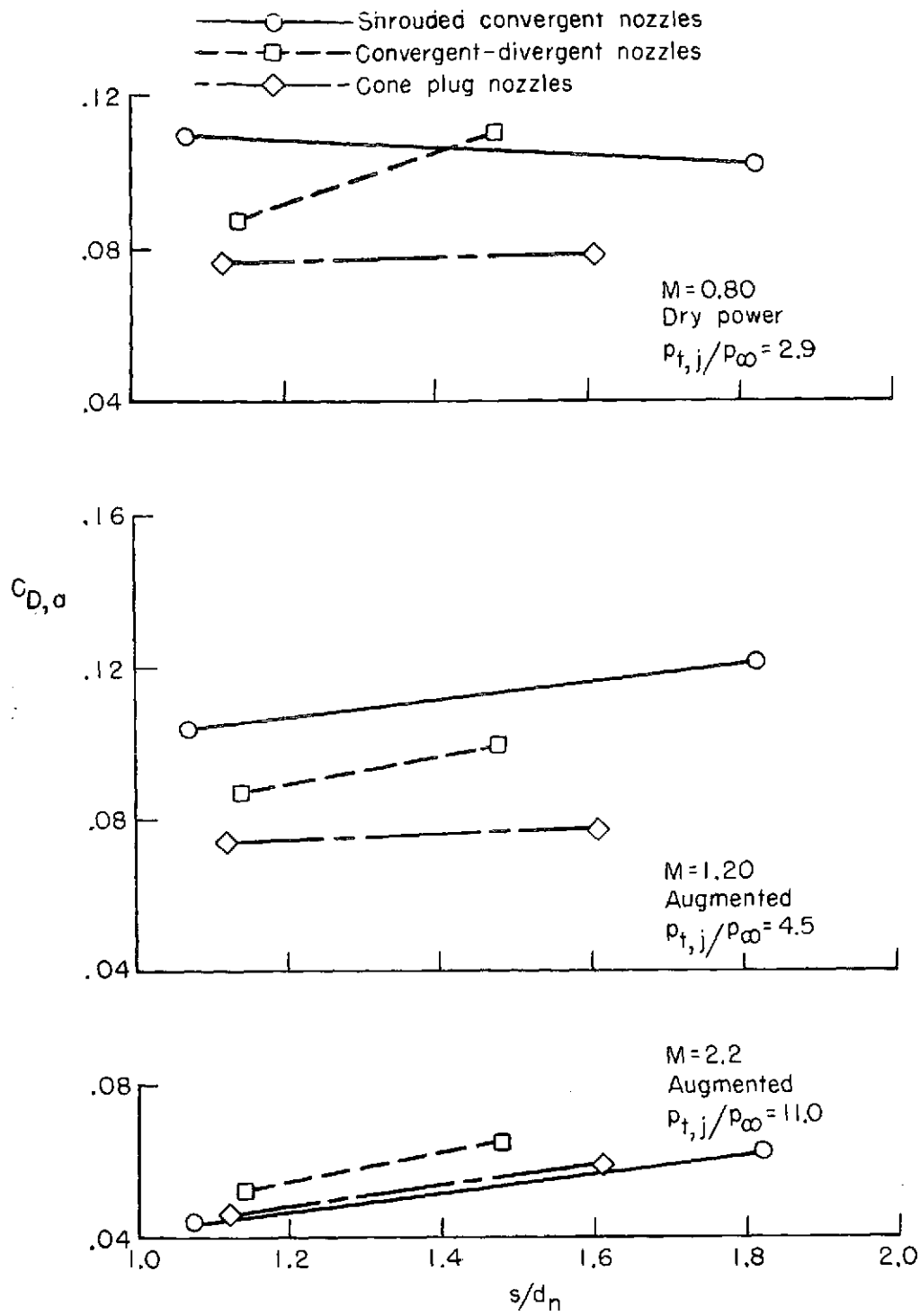

Figure 21.- Effect of engine lateral spacing on afterbody drag.

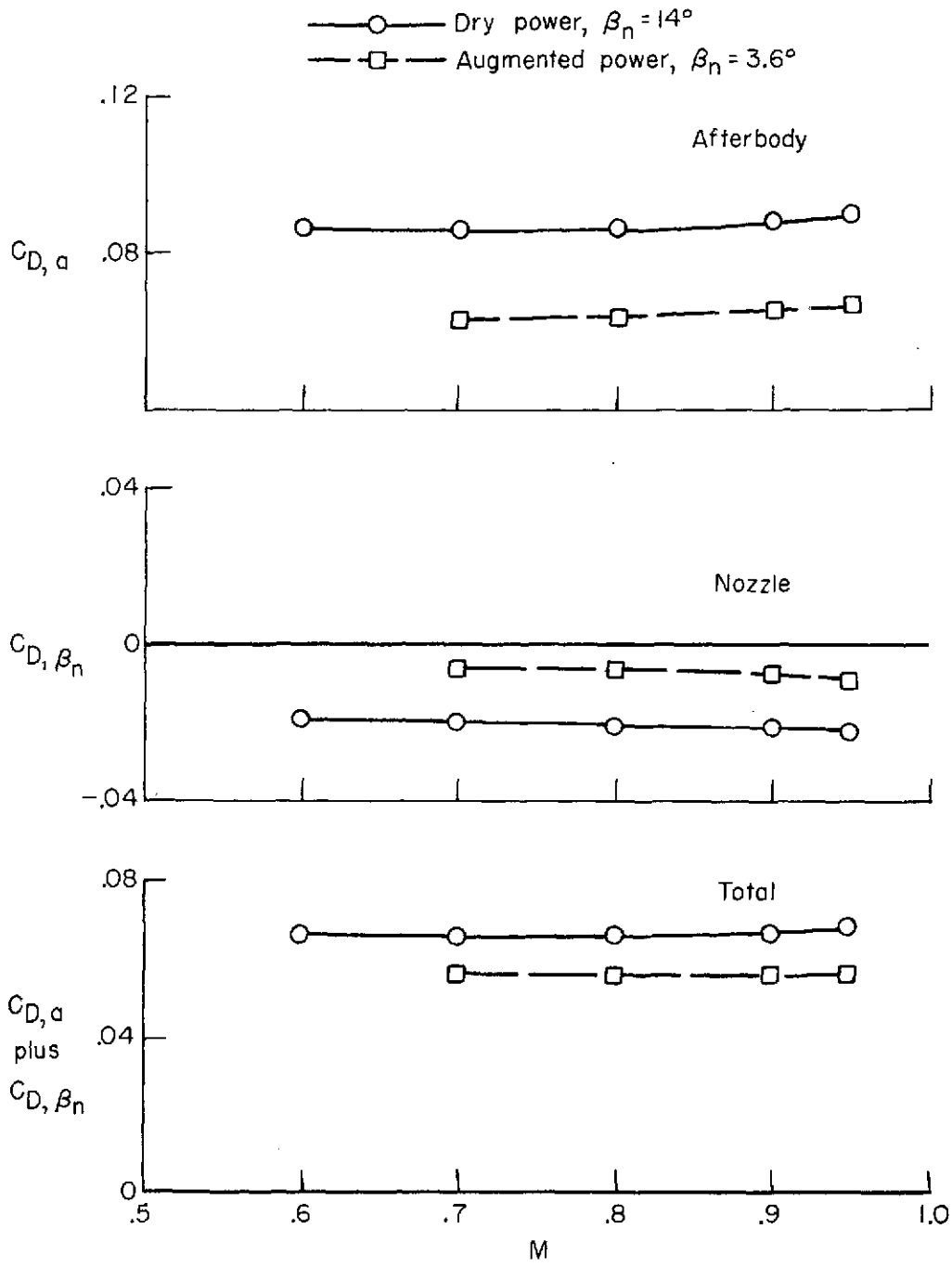

Figure 22.- Effect of nozzle configuration on afterbody performance. Elliptical interfairing with convergent-divergent nozzles.

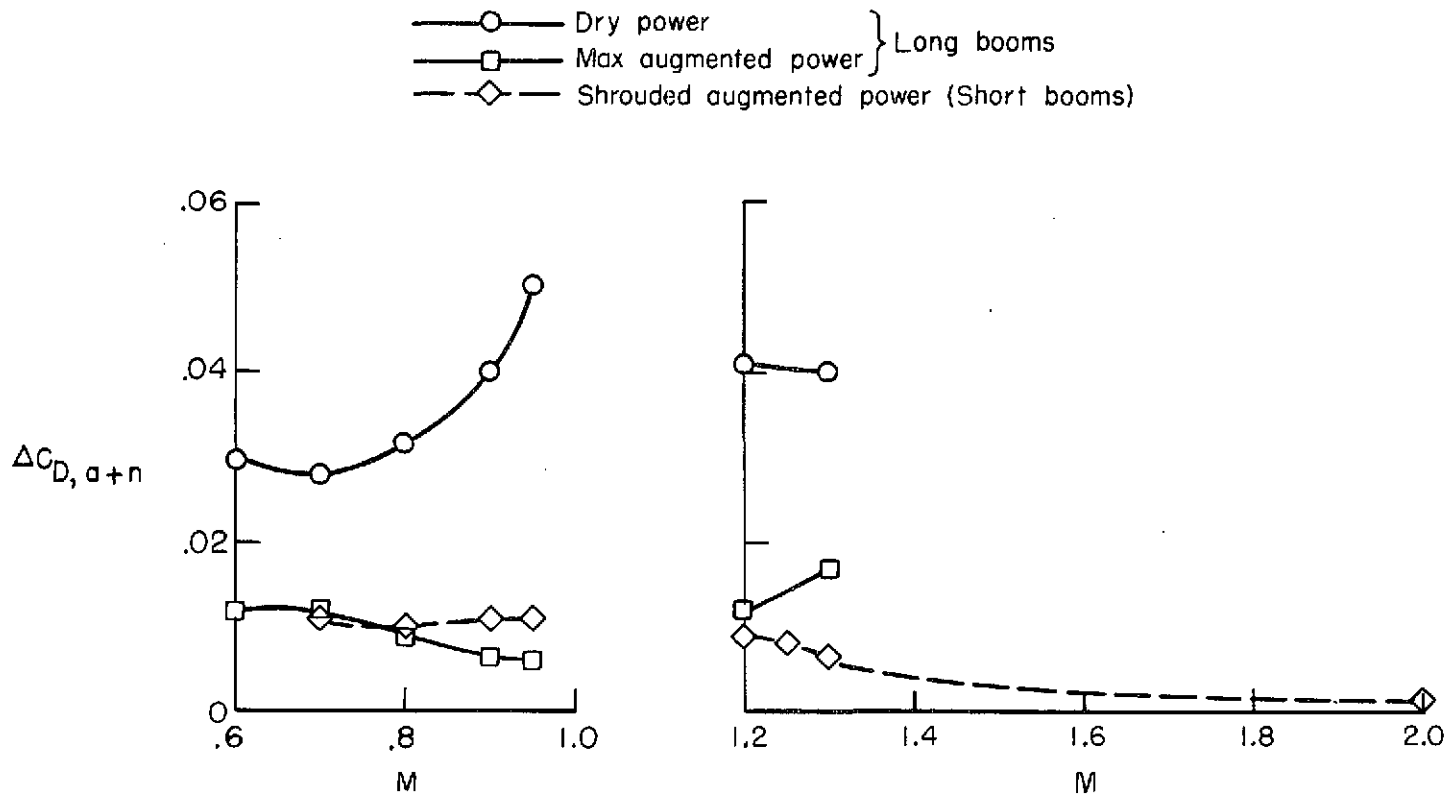

Figure 23.- Effect of addition of booms on total afterbody drag.

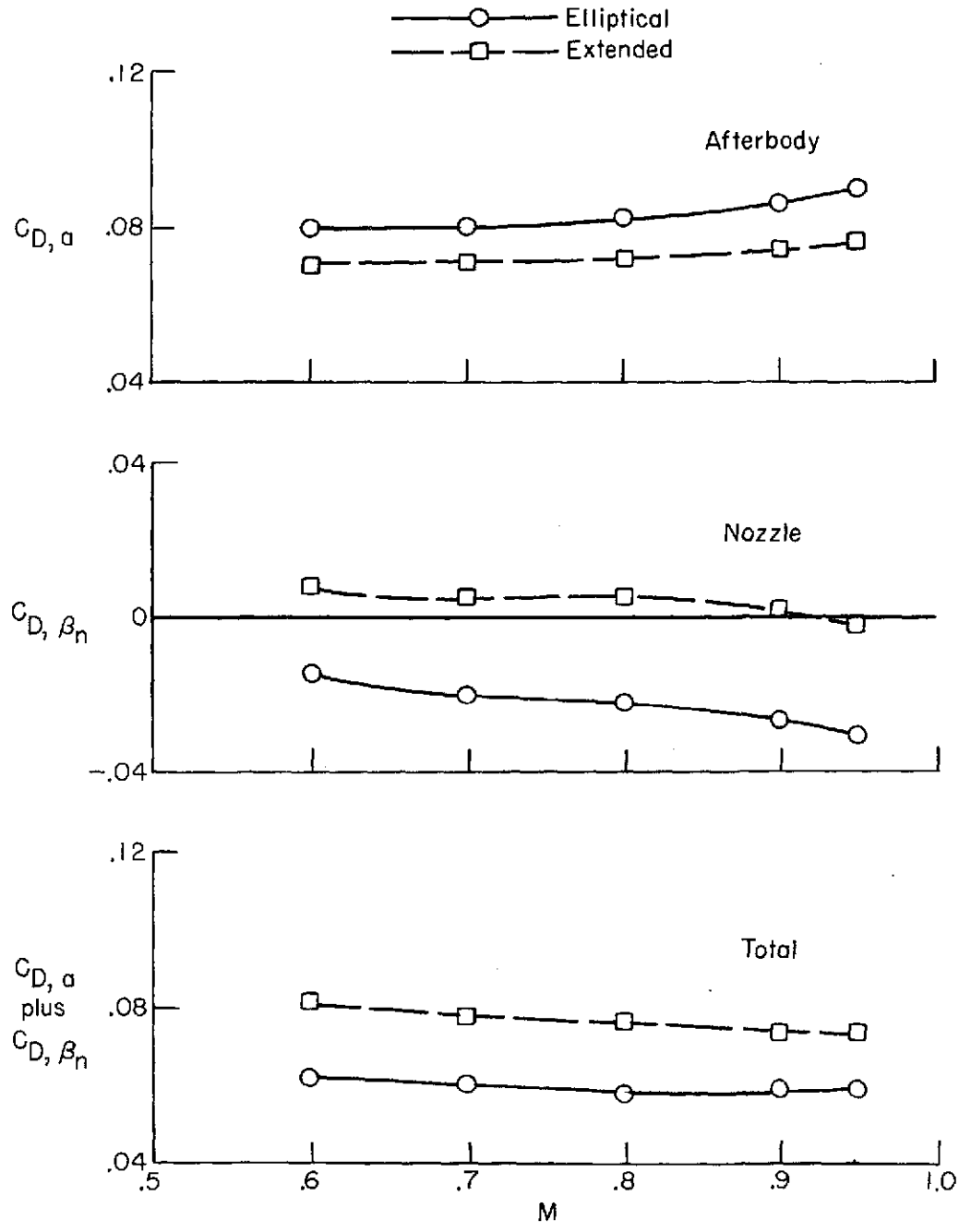

Figure 24.- Effect of interfairing shape on axial drag coefficients. Dry-power iris nozzles.

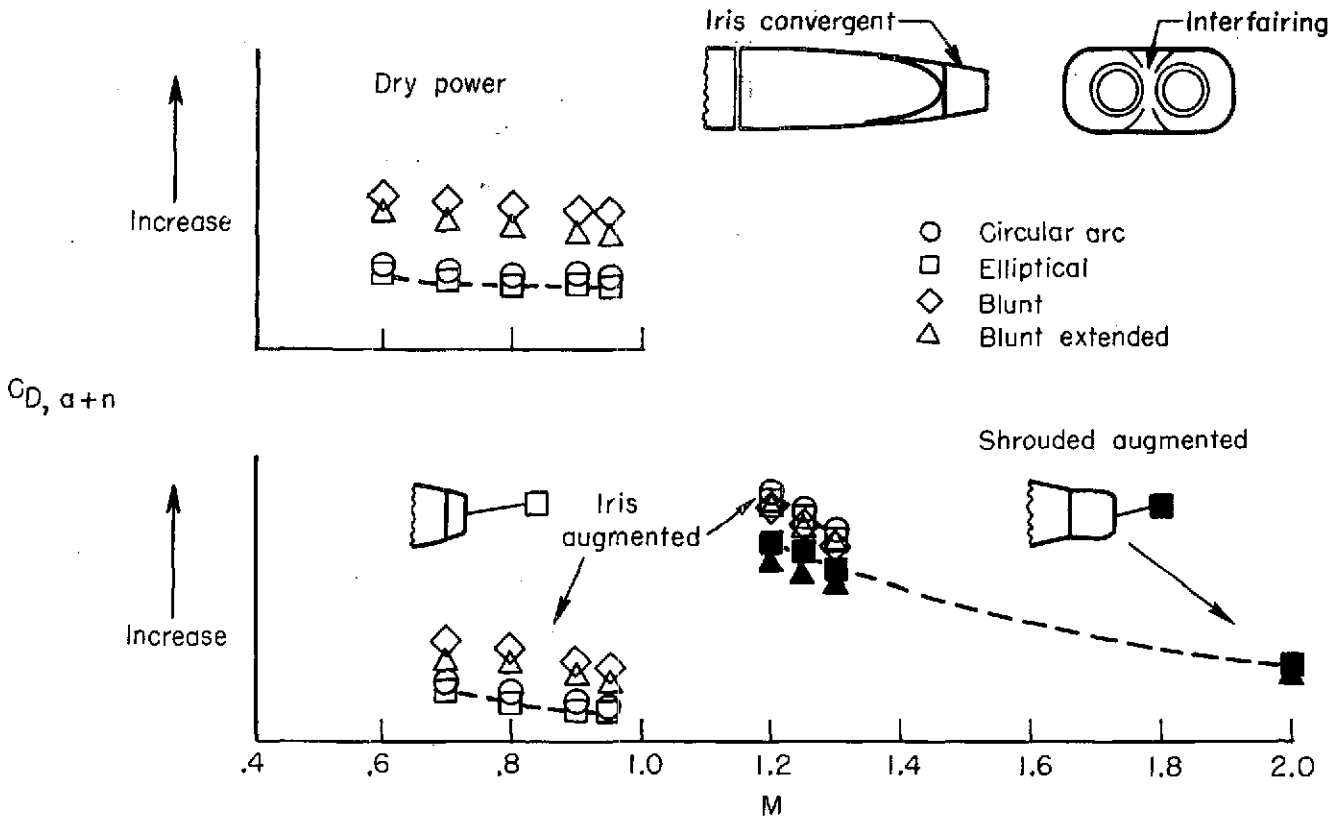

Figure 25.- Interfairing shape influence on afterbody-plus-nozzle drag coefficient.